The ScotoSinglet Model: A Scalar Singlet Extension of the Scotogenic Model

Ankit Beniwal,^a Juan Herrero-García,^b Nicholas Leerdam,^c Martin White^c and Anthony G. Williams^c

```
<sup>a</sup> Center for Cosmology, Particle Physics and Phenomenology (CP3),
Université catholique de Louvain, B-1348 Louvain-la-Neuve, Belgium
```

E-mail: ankit.beniwal@uclouvain.be, juan.herrero@ific.uv.es, nicholas.leerdam@adelaide.edu.au, martin.white@adelaide.edu.au, anthony.williams@adelaide.edu.au

ABSTRACT: The Scotogenic Model is one of the most minimal models to account for both neutrino masses and dark matter (DM). In this model, neutrino masses are generated at the one-loop level, and in principle, both the lightest fermion singlet and the lightest neutral component of the scalar doublet can be viable DM candidates. However, the correct DM relic abundance can only be obtained in somewhat small regions of the parameter space, as there are strong constraints stemming from lepton flavour violation, neutrino masses, electroweak precision tests and direct detection. For the case of scalar DM, a sufficiently large lepton-number-violating coupling is required, whereas for fermionic DM, coannihilations are typically necessary. In this work, we study how the new scalar singlet modifies the phenomenology of the Scotogenic Model, particularly in the case of scalar DM. We find that the new singlet modifies both the phenomenology of neutrino masses and scalar DM, and opens up a large portion of the parameter space of the original model.

Keywords: Neutrino Physics, Dark Matter, Beyond the Standard Model, Lepton Flavor Violation, Radiative Models.

ARXIV EPRINT: 2010.05937

b Departamento de Física Teórica and IFIC, Universidad de Valencia-CSIC,
 C/ Catedrático José Beltrán, 2, E-46980 Paterna, Spain

^cARC Centre of Excellence for Dark Matter Particle Physics and CSSM, Department of Physics, University of Adelaide, SA 5005, Australia

Co	ontents			
1	Introduction			
2	The ScotoSinglet Model (ScSM)	3		
3	Phenomenology	5		
	3.1 Naturalness, perturbativity and \mathbb{Z}_2 symmetry breaking	6		
	3.1.1 Perturbativity	6		
	3.1.2 Naturalness	6		
	3.1.3 \mathbb{Z}_2 symmetry breaking at tree-level	6		
	3.2 Neutrino masses	7		
	3.3 Integrating-out the heavy scalar singlet	8		
	3.4 Electroweak precision tests	9		
	3.5 Higgs decay into di-photons	10		
	3.6 Lepton flavour violation	11		
	3.7 Relic abundance	11		
	3.8 Direct detection	12		
	3.9 \mathbb{Z}_2 symmetry at high energies	13		
4	Numerical analysis	13		
5	Results	16		
	5.1 No mixing case: Scotogenic model + scalar singlet	16		
	5.2 DM candidate: real scalar, η_2	17		
	5.3 DM candidate: real pseudoscalar, A	21		
	5.4 DM candidate: Majorana fermion, ψ_2	21		
6	Conclusions	22		
A	Mass eigenstate basis	23		
В	Parameterisation of the Yukawa couplings	25		
\mathbf{C}	Potential stability	27		
D	Renormalisation Group Equations (RGEs)	27		
	D.1 Gauge couplings	28		
	D.2 Quartic scalar couplings	28		
	D.3 Yukawas, masses and trilinear couplings	29		

1 Introduction

The origin of light neutrino masses and dark matter (DM) remain unsolved puzzles of the Standard Model (SM). Many explanations have been proposed; of particular interest are those that can simultaneously account for both of them. A successful model should not only provide a natural explanation for the smallness of neutrino masses, it should also include a viable DM candidate. For the former case, radiative neutrino mass models (see refs. [1, 2] for a review), with new states at the TeV scale, are an attractive solution. As for DM, a GeV-TeV scale Weakly Interacting Massive Particle, stabilised by some remanent symmetry (e.g., \mathbb{Z}_2), provides an elegant solution. In this context, the Scotogenic Model (ScM), first proposed by Ernest Ma (2006) [3] (see also refs. [4-21]), emerges as one of the simplest joint solutions for neutrino masses and DM. It adds a new scalar doublet Φ and new Majorana singlets ψ_i ($i \geq 2$), all of them charged under a \mathbb{Z}_2 symmetry. Another interesting variant has been recently proposed where the \mathbb{Z}_2 symmetry is exchanged for a U(1) symmetry; it is referred to as the Generalised Scotogenic Model (GScM) [22].

In the ScM, neutrino masses are generated at the one-loop level, and are proportional to a particular quartic coupling, $\lambda_{H\Phi,3}$, and the Majorana masses, m_{ψ_i} . In principle, DM can either be in the form of the lightest ψ_i , or the lightest neutral component of Φ (either CP-even or CP-odd, depending on the sign of $\lambda_{H\Phi,3}$). In both cases, however, saturating the observed DM relic abundance is non-trivial as the models are subject to strong constraints from neutrino masses, electroweak precision tests (EWPT), direct detection (DD) experiments, and particularly lepton flavour violation (LFV) processes; the DD limits, however, can be circumvented by imposing a lower bound on the splitting between the CP-even and CP-odd scalars, i.e., a lower bound on $\lambda_{H\Phi,3}$. For the fermion DM case, coannihilations are typically required [22].

In this work, we investigate how the parameter space of the original ScM is augmented in the presence of a real scalar singlet, denoted by φ . This can be understood as the simplest extension of the Scotogenic model [3], which we refer to as the ScotoSinglet Model (ScSM). Notice that the usual ScM is recovered in the limit of no mixing, and when the singlet decouples. The model was first outlined in ref. [23], assuming an MeV-scale scalar DM with annihilations into neutrinos only (see also ref. [24], based on the one-loop classification of ref. [25]). A scale-invariant version of the ScM with an extra scalar singlet was studied in ref. [14]. A similar singlet-doublet model², also in the fermion sector, was studied in ref. [27]; for other studies, see refs. [28–30]. Collider signatures of a similar model (without the λ_5 term) were studied in ref. [31]. Low-scale leptogenesis was studied in the context of ScM [32] and a real scalar singlet [33]. Recently, in ref. [34], inflation was studied in a ScM with an additional scalar singlet (not charged under the \mathbb{Z}_2 symmetry). Also recently, a different variant of the ScM with a scalar singlet not charged under \mathbb{Z}_2 and spontaneously broken lepton number was studied in ref. [35]. Here we aim to provide a more detailed analysis of the full parameter space while focusing on all possible DM candidates in the

¹In this case, the scalar singlet is not charged under a \mathbb{Z}_2 symmetry, and instead plays the role of a dilaton with very different phenomenological implications.

²A singlet-triplet DM model with radiative neutrino masses is proposed in ref. [26].

ScSM, and comparing our results against the usual ScM. We also study how the parameter space expands with respect to the case of pure singlet or pure doublet DM via turning on/off the relevant couplings.

The ScSM has some interesting features (mostly due to the presence of a scalar singlet-doublet mixing, and a trilinear coupling between φ , Φ and the Higgs doublet H): new contributions to neutrino masses, 3 potential DM candidates (one of which is a mixture of singlet and doublet), and the possibility to maintain the \mathbb{Z}_2 symmetry up to high energy scales. In light of these features, we perform, for the first time, a convergent global fit of the ScSM. As we will show, the presence of the singlet significantly opens up the allowed parameter space of the CP-even scalar DM, which now has a non-negligible singlet component. Due to the presence of the trilinear coupling with the singlet, there exists a splitting between the CP-even components. This naturally translates into a significant mass splitting between the lightest CP-even and CP-odd scalars, which allows to naturally evade the stringent DD limits.

The rest of the paper is organised as follows. In section 2, we introduce the ScSM.³ The phenomenology of the ScSM and various theoretical/observational constraints that we impose are described in section 3. Sections 4 and 5 are devoted to our numerical analysis and results, respectively. Our conclusions are presented in section 6. A list of appendices provide supplementary information for understanding various expressions in the paper.

2 The ScotoSinglet Model (ScSM)

The new particle fields of the ScSM and their quantum numbers are presented in table 1. The Lagrangian for the Majorana fermion fields $\Psi \equiv (\psi_1, \dots, \psi_N)^T$ is given by

$$\mathcal{L}_{\Psi} = \frac{1}{2} \overline{\Psi} (i \partial \!\!\!/ - M_{\Psi}) \Psi - \overline{\Psi} \mathbf{y}_{\Psi} \, \tilde{\Phi}^{\dagger} L + \text{H.c.}, \qquad (2.1)$$

where M_{Ψ} is an $N \times N$ diagonal mass matrix with real and positive values, and \mathbf{y}_{Ψ} is an $N \times 3$ complex matrix of Yukawa couplings. Without loss of generality, we take $m_{\psi_1} \geq m_{\psi_2} \geq \ldots \geq m_{\psi_N}$. To reproduce the neutrino masses, $N \geq 2$. Here we study the minimal case (N = 2).

The most general form of a \mathbb{Z}_2 symmetric scalar potential is

$$V = -\mu_H^2 H^{\dagger} H + \lambda_H (H^{\dagger} H)^2 + m_{\Phi}^2 \Phi^{\dagger} \Phi + \lambda_{\Phi} (\Phi^{\dagger} \Phi)^2 + \frac{1}{2} m_{\varphi}^2 \varphi^2 + \frac{1}{4} \lambda_{\varphi} \varphi^4$$

$$+ \lambda_{H\Phi,1} (H^{\dagger} H) (\Phi^{\dagger} \Phi) + \lambda_{H\Phi,2} (H^{\dagger} \Phi) (\Phi^{\dagger} H) + \frac{1}{2} \left[\lambda_{H\Phi,3} (H^{\dagger} \Phi)^2 + \text{H.c.} \right]$$

$$+ \frac{1}{2} \lambda_{H\varphi} H^{\dagger} H \varphi^2 + \frac{1}{2} \lambda_{\Phi\varphi} \Phi^{\dagger} \Phi \varphi^2 + \left[\kappa \Phi^{\dagger} H \varphi + \text{H.c.} \right]. \tag{2.2}$$

 $^{^3\}mathrm{Our}$ FeynRules [36] and CalcHEP [37] model files are available here.

⁴For the main purpose of our study (scalar DM and comparison with the ScM), the results are not expected to change significantly for N > 2.

Fields	$SU(3)_C$	$SU(2)_L$	$U(1)_Y$	\mathbb{Z}_2
Real φ	1	1	0	_
Φ	1	2	1/2	_
ψ_k	1	1	0	_

Table 1: Particle content of the ScotoSinglet Model (ScSM). Here k = 1, ..., N are the number of new Majorana fermion fields; in our study, we consider N = 2.

Here $H \equiv (0, (v+h)/\sqrt{2})^T$ is the SM Higgs doublet after electroweak symmetry breaking (EWSB).⁵ Without loss of generality, $\lambda_{H\Phi,3}$ can be made real by performing a rotation of Φ . Although κ , in general, can be complex, we also take it as real in our study.

We assume that the \mathbb{Z}_2 symmetry is exactly preserved such that in the vacuum state, $\langle \Phi \rangle = \langle \varphi \rangle = 0$. The electrically neutral and charged field components of the weak scalar doublet Φ are

$$\Phi \equiv \begin{pmatrix} \phi^+ \\ \frac{1}{\sqrt{2}} \left(\phi_R + iA \right) \end{pmatrix} . \tag{2.3}$$

After EWSB, the physical masses of charged scalar ϕ^+ and CP-odd pseudoscalar A are

$$m_{\phi^+}^2 = m_{\Phi}^2 + \frac{1}{2}\lambda_{H\Phi,1}v^2$$
, (2.4a)

$$m_A^2 = m_{\Phi}^2 + \frac{1}{2}(\lambda_{H\Phi,1} + \lambda_{H\Phi,2} - \lambda_{H\Phi,3})v^2$$
. (2.4b)

In the (ϕ_R, φ) basis, the squared mass matrix is non-diagonal, namely

$$\mathcal{M}^{2} = \begin{pmatrix} \frac{\partial^{2} V}{\partial \phi_{R}^{2}} & \frac{\partial^{2} V}{\partial \phi_{R} \partial \varphi} \\ \frac{\partial^{2} V}{\partial \varphi \partial \phi_{R}} & \frac{\partial^{2} V}{\partial \varphi^{2}} \end{pmatrix} = \begin{pmatrix} a & c \\ c & b \end{pmatrix}, \qquad (2.5)$$

 $where^{6}$

$$a = m_{\Phi}^2 + \frac{1}{2}(\lambda_{H\Phi,1} + \lambda_{H\Phi,2} + \lambda_{H\Phi,3})v^2, \quad b = m_{\varphi}^2 + \frac{1}{2}\lambda_{H\varphi}v^2, \quad c = \kappa v.$$
 (2.6)

Notice from eq. (2.2) that κ controls the mixing between ϕ_R and φ , and $\lambda_{H\Phi,3}$ the mass splitting between ϕ_R and A. To diagonalise the mass matrix in eq. (2.5), we perform a rotation into the physical mass basis (η_1, η_2) by

$$\begin{pmatrix} \eta_1 \\ \eta_2 \end{pmatrix} = \begin{pmatrix} \cos \theta & \sin \theta \\ -\sin \theta & \cos \theta \end{pmatrix} \begin{pmatrix} \phi_R \\ \varphi \end{pmatrix} , \qquad (2.7)$$

⁵The SM Higgs boson mass is $m_h = \sqrt{2 \lambda_H v^2} = \sqrt{2 \mu_H^2} = 125 \,\text{GeV}$, where the vacuum expectation value is $v = \sqrt{\mu_H^2/\lambda_H} = 246.22 \,\text{GeV}$.

⁶Notice that $m_A^2 = a - \lambda_{H\Phi,3}v^2$, where a is the mass of the CP-even scalar doublet in the absence of mixing $(\theta = 0)$.

such that

$$\tan 2\theta = \frac{2c}{a-b} \,. \tag{2.8}$$

The mixing angle $\theta \in [0, \pi]$ and the quadrant is determined by the signs of a - b and c. For instance, a - b > 0 and c > 0 implies $\theta \in (0, \pi/4)$, whereas a - b < 0 and c > 0 implies $\theta \in (\pi/4, \pi/2)$. The physical scalar $\eta_{1,2}$ masses are given by

$$m_{\eta_1}^2 = \frac{1}{2} \left(a + b + \sqrt{(a-b)^2 + 4c^2} \right),$$
 (2.9a)

$$m_{\eta_2}^2 = \frac{1}{2} \left(a + b - \sqrt{(a-b)^2 + 4c^2} \right).$$
 (2.9b)

Note that by convention, $m_{\eta_1} \geq m_{\eta_2}$. The DM candidate can either be the CP-even scalar η_2 , the CP-odd pseudoscalar A or the lightest Majorana fermion ψ_2 (as $m_{\psi_1} \geq m_{\psi_2}$ by convention).

3 Phenomenology

After EWSB and rotation into the physical mass basis, the ScSM contains 12 free model parameters, namely

5 masses (1 mixing angle):
$$\{m_{\psi_1}, m_{\psi_2}, m_{\eta_1}, m_{\eta_2}, m_A, \theta\},$$
 (3.1a)

6 couplings:
$$\{\lambda_{\Phi}, \lambda_{\varphi}, \lambda_{H\Phi,1}, \lambda_{H\Phi,2}, \lambda_{H\varphi}, \lambda_{\Phi\varphi}\}$$
. (3.1b)

The remaining parameters in eq. (2.2) can be expressed as (see appendix A)

$$m_{\Phi}^2 = m_{\eta_1}^2 \cos^2 \theta + m_{\eta_2}^2 \sin^2 \theta - \frac{1}{2} \left(\lambda_{H\Phi,1} + \lambda_{H\Phi,2} + \lambda_{H\Phi,3} \right) v^2, \qquad (3.2a)$$

$$m_{\varphi}^2 = m_{\eta_1}^2 \sin^2 \theta + m_{\eta_2}^2 \cos^2 \theta - \frac{1}{2} \lambda_{H\varphi} v^2,$$
 (3.2b)

$$m_{\phi^+}^2 = m_{\Phi}^2 + \frac{1}{2} \lambda_{H\Phi,1} v^2 ,$$
 (3.2c)

$$\lambda_{H\Phi,3} = \frac{1}{v^2} \left(m_{\eta_1}^2 \cos^2 \theta + m_{\eta_2}^2 \sin^2 \theta - m_A^2 \right) , \qquad (3.2d)$$

$$\kappa = \frac{1}{v} (m_{\eta_1}^2 - m_{\eta_2}^2) \sin \theta \cos \theta.$$
 (3.2e)

We also have free parameters within the complex Yukawa matrices, for which we use a Casas-Ibarra parametrisation [38]. For N=2 fermionic singlets, there are N=2 real angles from the complex orthogonal Casas-Ibarra matrix R, and N-1=1 Majorana phase in the PMNS matrix U (as one of the neutrinos is massless); see appendix B for more details. Thus, we can express the 6 complex Yukawa couplings in terms of the low-energy neutrino oscillation data (3 masses, 3 angles, and 2 phases), the 2 heavy Majorana masses parameters, and the 2 real angles of the R matrix. These are considered as nuisance parameters in our study.

In the following subsections, we discuss various theoretical/observational constraints that are imposed on the allowed model parameter space.

3.1 Naturalness, perturbativity and \mathbb{Z}_2 symmetry breaking

3.1.1 Perturbativity

From perturbativity arguments, we require all quartic couplings in the potential to satisfy

$$|\lambda_i| < 4\pi \,. \tag{3.3}$$

In addition, we also impose the co-positivity conditions discussed in appendix C. As for the Yukawa couplings (derived parameters in our scan), we require

$$|y_{yy}^{\alpha}|^2 < 4\pi \,, \tag{3.4}$$

where i = 1, 2 and $\alpha = e, \mu, \tau$.

3.1.2 Naturalness

Using eq. (2.8) and expressing everything in terms of the physical scalar masses, the trilinear coupling κ can be bounded as

$$c \equiv \kappa v = (m_{\eta_1}^2 - m_{\eta_2}^2) \sin \theta \cos \theta \Longrightarrow |\kappa| \lesssim \frac{m_{\eta_1}^2}{2v} , \qquad (3.5)$$

where we have used $m_{\eta_1}^2 \gg m_{\eta_2}^2$ in the last step. However, as the heavy neutral scalar masses are unknown, this upper bound is not very useful.

We can make use of the fact that the trilinear coupling gives a correction to the Higgs boson mass at the one-loop level, where the new scalars run in the loop. Up to factors of 2 and logs, we estimate

$$m_h^2 \gtrsim \frac{|\kappa|^2}{16\pi^2} \,. \tag{3.6}$$

For the fine-tuning to be under control, i.e., $\delta m_h/m_h < \epsilon$, we demand that

$$|\kappa| \lesssim 4\pi\epsilon \, m_h \simeq 1.5 \,\text{TeV} \,,$$
 (3.7)

where we have assumed $\epsilon \simeq 1$. Similar considerations were made in the Zee model [39]. If the fine-tuning condition is relaxed (i.e., $\epsilon \gtrsim 1$), the upper limit on κ can also be relaxed.

3.1.3 \mathbb{Z}_2 symmetry breaking at tree-level

If $|\kappa|$ is much larger than the scalar masses, it can lead to a deeper minimum than the SM one, thereby breaking the \mathbb{Z}_2 symmetry. Looking at different field directions, and using eq. (3.3), we get

$$|\kappa| \lesssim \mathcal{O}(1) \left(-\mu_H^2 + m_\Phi^2 + m_\varphi^2 \right).$$
 (3.8)

The above requirement, although more robust than the naturality one in eq. (3.7), turns out to be weaker, particularly for m_{Φ} and m_{φ} larger than the EW scale. In order for the model to be valid above the EW scale (such that the \mathbb{Z}_2 symmetry is preserved), it is important to check that the RGE evolution does not only preserve $m_{\Phi}^2 > 0$ and $m_{\varphi}^2 > 0$, but also that $|\kappa|$ is not too large compared to the rest of the scalar masses. The latter requirement, however, is expected to be easily satisfied, as κ renormalises multiplicatively (see section 3.9).

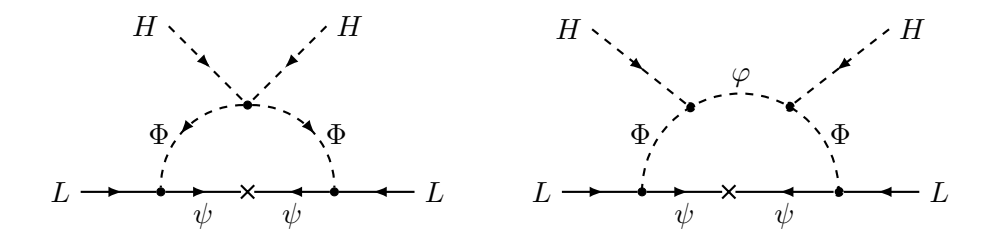


Figure 1: Feynman diagrams for the neutrino masses at the one-loop level. The left panel shows the contribution in the Scotogenic Model (proportional to $\lambda_{H\Phi,3}$), whereas the right panel shows the new contribution in the ScotoSinglet Model (ScSM) (proportional to κ^2).

3.2 Neutrino masses

Neutrino masses are generated at the one-loop level with the neutral fields running in the loop, see figure 1. From the Yukawa Lagrangian, eq. (2.1), and the scalar potential, eq. (2.2), we can see that the lepton number is violated by 2 units in the presence of \mathbf{y}_{Ψ} , M_{Ψ} and either:

- 1. The quartic coupling $\lambda_{H\Phi,3}$. This contribution is same as in the ScM; see the left diagram in figure 1.
- 2. The square of the dimensionful trilinear coupling, κ^2 . This is the new contribution in the ScSM; see the right diagram in figure 1.

These are the parameter combinations that enter in the expression for the neutrino masses, namely⁷

$$(M_{\nu})_{\alpha\beta} = \sum_{k=1}^{2} \frac{y_{k\alpha} m_{\psi_k} y_{k\beta}}{32\pi^2} \left[\cos^2 \theta \, F_k(m_{\eta_1}) + \sin^2 \theta \, F_k(m_{\eta_2}) - F_k(m_A) \right] \,, \tag{3.9}$$

where the loop function is

$$F_k(m_x) = \frac{m_x^2}{m_x^2 - m_{\psi_k}^2} \log\left(\frac{m_x^2}{m_{\psi_k}^2}\right). \tag{3.10}$$

It is instructive to expand in the limit of small $\lambda_{H\Phi,3}$ and κ . For a > b and small κ , the mixing is $\theta \approx 0$, thus $\eta_1(\eta_2)$ is mostly doublet (singlet). In this case, the mass splitting between η_1 and A reads $m_{\eta_1}^2 - m_A^2 \approx \lambda_{H\Phi,3} v^2$. For $m_{\eta_1} > m_{\eta_2} \gg m_{\psi_k}$, we find that

$$(M_{\nu})_{\alpha\beta} \approx \sum_{k=1}^{2} \frac{y_{k\alpha} m_{\psi_k} y_{k\beta}}{32\pi^2} \left[\frac{\lambda_{H\Phi,3} v^2}{m_{\eta_1}^2} - \frac{\kappa^2 v^2}{(m_{\eta_1^2} - m_{\eta_2}^2)^2} \log\left(\frac{m_{\eta_1}^2}{m_{\eta_2}^2}\right) \right]. \tag{3.11}$$

⁷We believe there are two typos in the expressions of ref. [23]: i) a factor of π is missing in the denominator; and ii) an extra contribution to the scalar masses after EWSB is missing – this is due to the $\lambda_{H\Phi,1}$ term in the potential (λ_4 in the notation of ref. [23]).

For $m_{\eta_1} \gg m_{\psi_k} \gg m_{\eta_2}$, we get

$$(M_{\nu})_{\alpha\beta} \approx \sum_{k=1}^{2} \frac{y_{k\alpha} m_{\psi_k} y_{k\beta}}{32\pi^2} \left[\frac{\lambda_{H\Phi,3} v^2}{m_{\eta_1}^2} - \frac{\kappa^2 v^2}{m_{\eta_1}^4} \log \left(\frac{m_{\eta_1}^2}{m_{\psi_k}^2} \right) \right].$$
 (3.12)

Alternatively, for b > a, $\theta \approx \pi/2$ and thus $\eta_1(\eta_2)$ is mostly singlet (doublet). The mass splitting between η_2 and A is $m_{\eta_2}^2 - m_A^2 \approx \lambda_{H\Phi,3} v^2$. For $m_{\eta_1} > m_{\eta_2} \gg m_{\psi_k}$, we get

$$(M_{\nu})_{\alpha\beta} \approx \sum_{k=1}^{2} \frac{y_{k\alpha} m_{\psi_k} y_{k\beta}}{32\pi^2} \left[\frac{\lambda_{H\Phi,3} v^2}{m_{\eta_2}^2} + \frac{\kappa^2 v^2}{(m_{\eta_1^2} - m_{\eta_2}^2)^2} \log\left(\frac{m_{\eta_1}^2}{m_{\eta_2}^2}\right) \right], \tag{3.13}$$

whereas for $m_{\eta_1} \gg m_{\psi_k} \gg m_{\eta_2}$, we get

$$(M_{\nu})_{\alpha\beta} \approx \sum_{k=1}^{2} \frac{y_{k\alpha} m_{\psi_k} y_{k\beta}}{32\pi^2} \left\{ \frac{\lambda_{H\Phi,3} v^2}{m_{\psi_k}^2} \left[\log \left(\frac{m_{\psi_k}^2}{m_{\eta_2}^2} \right) - 1 \right] + \frac{\kappa^2 v^2}{m_{\eta_1}^4} \log \left(\frac{m_{\eta_1}^2}{m_{\psi_k}^2} \right) \right\}. \quad (3.14)$$

Note how the Scotogenic-like contribution (proportional to $\lambda_{H\Phi,3} v^2$) is always suppressed by the fermion or doublet mass, depending on which one is the heaviest state in the spectrum.

3.3 Integrating-out the heavy scalar singlet

If the singlet φ is the heaviest particle in the spectrum, e.g., $m_{\varphi}^2 \gg m_{\Phi}^2$ $(b \gg a)$, it can be integrated out (see ref. [40] for a similar study, and ref. [41] for the example of a charged scalar singlet). For scalar DM and $\theta \simeq \pi/2$, the DM candidate η_2 is mainly doublet and this is a good approximation. Assuming that the weak and mass eigenstates are similar, i.e., for small mixing (small θ), after integrating out the singlet at tree-level before EWSB, we obtain the following expression for the scalar potential at dimension-6:

$$V_{\text{eff}}(H,\Phi) = \left(\lambda_{H\Phi,2} - \frac{|\kappa|^2}{m_{\varphi}^2}\right) |H^{\dagger}\Phi|^2 + \frac{1}{2} \left[\left(\lambda_{H\Phi,3} - \frac{(\kappa^{\dagger})^2}{m_{\varphi}^2}\right) (H^{\dagger}\Phi)^2 + \text{H.c.} \right]$$

$$- \frac{\lambda_{H\varphi} |\kappa|^2}{m_{\varphi}^4} |H^{\dagger}\Phi|^2 H^{\dagger}H - \frac{\lambda_{\Phi\varphi} |\kappa|^2}{m_{\varphi}^4} |H^{\dagger}\Phi|^2 \Phi^{\dagger}\Phi$$

$$- \frac{1}{2} \left(\frac{\lambda_{H\varphi} (\kappa^{\dagger})^2}{m_{\varphi}^4} (H^{\dagger}\Phi)^2 H^{\dagger}H + \text{H.c.} \right)$$

$$- \frac{1}{2} \left(\frac{\lambda_{\Phi\varphi} (\kappa^{\dagger})^2}{m_{\varphi}^4} (H^{\dagger}\Phi)^2 \Phi^{\dagger}\Phi + \text{H.c.} \right). \tag{3.15}$$

After EWSB, the effective coupling $\frac{1}{2} \left[\lambda_{H\Phi,3}^{\text{eff}} (H^{\dagger}\Phi)^2 + \text{H.c.} \right]$ that appears in the neutrino masses is

$$\lambda_{H\Phi,3}^{\text{eff}} \equiv \lambda_{H\Phi,3} - \frac{(\kappa^{\dagger})^2}{m_{\varphi}^2} - \lambda_{H\varphi} \frac{(\kappa^{\dagger})^2}{m_{\varphi}^4} \frac{v^2}{2} \,. \tag{3.16}$$

This agrees with our expectation from considerations of lepton number violation. We see that neutrino masses can be suppressed either by small $\lambda_{H\Phi,3}$ and κ , or by cancellations

among these terms. Notice that the last term in eq. (3.16) gives a contribution to neutrino masses via a dimension-7 Weinberg-like operator, which is expected to be suppressed compared to the usual dimension-5 one (the rest of the terms). In our numerical scan, we check that the combination in eq. (3.16) is indeed fixed (with the scale set by the neutrino masses).

Let us elaborate a bit more on the threshold corrections to $\lambda_{H\Phi,2}$ and $\lambda_{H\Phi,3}$ at the scale of the singlet φ . Interestingly, the threshold effects increase their values for high energies. The stability conditions, however, must to be applied differently above and below m_{φ} . This effect has been used to keep the Higgs potential stable up to high energy scales in ref. [42]. Notice also that the signs of $\lambda_{H\Phi,3}$ and κ are preserved under the RGE flow due to their multiplicative renormalization. The behaviour in eq. (3.16) can also be understood from the scalar mass matrix, see eqs. (2.5) and (2.6). In the symmetric Higgs phase (scales above the EW scale) and for $m_{\varphi}^2 \gg m_{\Phi}^2$, the neutral scalar masses are see-saw like, i.e., from eqs. (2.9), we have

$$m_{\eta_1}^2 \simeq m_{\varphi}^2 + \frac{\kappa^2 v^2}{m_{\varphi}^2}, \quad m_{\eta_2}^2 \simeq m_{\Phi}^2 - \frac{\kappa^2 v^2}{m_{\varphi}^2}.$$
 (3.17)

We see that the lightest state (by convention η_2) is mainly doublet (Φ) , while the heaviest state (η_1) is mainly singlet (φ) , corresponding to a mixing angle of $\theta \approx \pi/2$. This repulsion of mass eigenvalues is the same effect that we see in the quartic couplings $\lambda_{H\Phi,2}$ and $\lambda_{H\Phi,3}$, see eq. (3.15).

3.4 Electroweak precision tests

The new particles in the ScSM contribute to the W^{\pm} and Z boson self-energies. These contributions are parametrised by the oblique S, T and U parameters [43, 44]. The strongest constraint comes from the T parameter, which bounds the mass splitting of the neutral and charged scalars. It is given by [45]

$$T = \frac{1}{16\pi^2 \alpha_{\rm em} v^2} \left[\cos^2 \theta \, \mathcal{F}(m_{\phi^+}^2, \, m_{\eta_1}^2) + \sin^2 \theta \, \mathcal{F}(m_{\phi^+}^2, \, m_{\eta_2}^2) + \mathcal{F}(m_{\phi^+}^2, \, m_A^2) \right.$$
$$\left. - \cos^2 \theta \, \mathcal{F}(m_{\eta_1}^2, \, m_A^2) - \sin^2 \theta \, \mathcal{F}(m_{\eta_2}^2, \, m_A^2) \right], \tag{3.18}$$

where the loop function (symmetric in x and y) is

$$\mathcal{F}(x^2, y^2) = \frac{x^2 + y^2}{2} - \frac{x^2 y^2}{x^2 - y^2} \ln\left(\frac{x^2}{y^2}\right). \tag{3.19}$$

The S parameter is given by

$$S = \frac{1}{\pi m_Z^2} \left[\cos^2 \theta \, \mathcal{B}_{22}(m_Z^2, \, m_{\eta_1}^2, \, m_A^2) + \sin^2 \theta \, \mathcal{B}_{22}(m_Z^2, \, m_{\eta_2}^2, \, m_A^2) - \mathcal{B}_{22}(m_Z^2, \, m_{\phi^+}^2, \, m_{\phi^+}^2) \right]. \tag{3.20}$$

Similarly, the combination S+U reads

$$S + U = \frac{1}{\pi m_W^2} \left[\cos^2 \theta \, \mathcal{B}_{22}(m_W^2, \, m_{\phi^+}^2, \, m_{\eta_1}^2) + \sin^2 \theta \, \mathcal{B}_{22}(m_W^2, \, m_{\phi^+}^2, \, m_{\eta_2}^2) \right.$$
$$\left. + \mathcal{B}_{22}(m_W^2, \, m_{\phi^+}^2, \, m_A^2) - 2 \, \mathcal{B}_{22}(m_W^2, \, m_{\phi^+}^2, \, m_{\phi^+}^2) \right], \tag{3.21}$$

where

$$\mathcal{B}_{22}(q^2, m_1^2, m_2^2) = B_{22}(q^2, m_1^2, m_2^2) - B_{22}(0, m_1^2, m_2^2). \tag{3.22}$$

The Passarino-Veltman function B_{22} [46] (symmetric in the last two arguments) is

$$B_{22}(q^2, m_1^2, m_2^2) = \frac{1}{4}(\Delta + 1)(m_1^2 + m_2^2 - \frac{1}{3}q^2) - \frac{1}{2} \int_0^1 X \ln(X - i\epsilon) \, \mathrm{d}x, \qquad (3.23)$$

where

$$X \equiv m_1^2 x + m_2^2 (1 - x) - q^2 x (1 - x), \quad \Delta \equiv \frac{2}{4 - d} + \ln 4\pi - \gamma_E, \qquad (3.24)$$

in d space-time dimensions and $\gamma_E \simeq 0.577$ is the Euler–Mascheroni constant. We use the compact analytic expressions from appendix B of ref. [39]. Our expressions agree with the ones for the Inert Doublet Model (IDM) [47] in the appropriate limits.

The oblique parameters are constrained from the global electroweak fit [48], assuming SM reference values of $m_h^{\rm ref}=125\,{\rm GeV}$ and $m_t^{\rm ref}=172.5\,{\rm GeV}$. The most recent fit gives

$$S = 0.04 \pm 0.11, \quad T = 0.09 \pm 0.14, \quad U = -0.02 \pm 0.11,$$
 (3.25)

along with the following correlation matrix:

$$\rho_{ij} = \begin{pmatrix}
1 & 0.92 & -0.68 \\
0.92 & 1 & -0.87 \\
-0.68 & -0.87 & 1
\end{pmatrix}.$$
(3.26)

3.5 Higgs decay into di-photons

The coupling between the SM Higgs h and charged scalar ϕ^+ in eq. (2.2) modifies the decay rate of the $h \to \gamma \gamma$ process. The ratio with respect to the SM value is [49–51]

$$\mathcal{R}_{\gamma\gamma} \equiv \frac{\Gamma(h \to \gamma\gamma)_{\text{ScSM}}}{\Gamma(h \to \gamma\gamma)_{\text{SM}}} = \left| 1 + \frac{\lambda_{H\Phi,1} v^2}{2m_{\phi^+}^2} \frac{A_0(\tau_{\phi^+})}{A_1(\tau_W) + \frac{4}{3} A_{1/2}(\tau_t)} \right|^2.$$
(3.27)

Here the loop functions $A_i(\tau_j \equiv 4m_j^2/m_h^2)$ read

$$A_0(x) = -x + x^2 f\left(\frac{1}{x}\right),$$
 (3.28a)

$$A_{1/2}(x) = 2x + 2x(1-x) f\left(\frac{1}{x}\right),$$
 (3.28b)

$$A_1(x) = -2 - 3x - 3x(2 - x) f\left(\frac{1}{x}\right),$$
 (3.28c)

where $j = \phi^+$, t and W, and $f = \arcsin^2(\sqrt{x})$ for $m_h < 2m_i$.

LFV process	Upper limit (90% CL)	Ref.
$\mu \to e \gamma$	4.2×10^{-13}	MEG [52]
$\tau \to \mu \gamma$	4.4×10^{-8}	PDG [53]
$\tau \to e \gamma$	3.3×10^{-8}	PDG [53]
$\mu \to 3e$	1.0×10^{-12}	PDG [53]
$ au ightarrow 3 \mu$	2.1×10^{-8}	PDG [53]
au ightarrow 3e	2.7×10^{-8}	PDG [53]
${\mu \to e \text{ (Au)}}$	7.0×10^{-13}	PDG [53]
$\mu \to e (\mathrm{Ti})$	4.3×10^{-12}	PDG [53]

Table 2: Upper limits on the branching ratios/conversion rates of various lepton flavour violation (LFV) processes at 90% CL. Here $\mu \to e$ refers to conversion rate in gold (Au) and titanium (Ti).

3.6 Lepton flavour violation

We use the usual expressions for the lepton flavour violation (LFV) processes (including $\mu - e$ conversion rates in various elements) that are applicable for the ScM [11, 22]. For instance, radiative decays are given by

$$\mathcal{BR}(\ell_{\alpha} \to \ell_{\beta} \gamma) = \frac{3 \alpha_{\text{em}}}{64\pi G_F^2 m_{\phi^+}^4} \left| \sum_{i} y_{i\beta}^* y_{i\alpha} F\left(\frac{m_{\psi_i}^2}{m_{\phi^+}^2}\right) \right|^2 \mathcal{BR}(\ell_{\alpha} \to \ell_{\beta} \nu_{\alpha} \overline{\nu_{\beta}}), \qquad (3.29)$$

where

$$F(x) = \frac{1 - 6x + 3x^2 + 2x^3 - 6x^2 \log x}{6(1 - x)^4}.$$
 (3.30)

The various LFV processes that we include in our study are summarised in table 2.

3.7 Relic abundance

The ScSM permits both scalar and fermionic DM candidates, but we focus on the case of scalar DM for two reasons:

- 1. The fermion DM case is very similar to the usual ScM where strong constraints from LFV exist on the Yukawa couplings. It requires special textures, and/or coannihilations and/or fermion triplets instead of singlets to saturate the observed DM abundance. In our scan, we indeed find the need for coannihilations (see section 5).
- 2. It is interesting to study the rich phenomenology of CP-even scalar DM (η_2) as an admixture of singlet (pure singlet case is $\theta \simeq 0$) and doublet (pure doublet case is $\theta \simeq \pi/2$) components, see eq. (2.7). The doublet case (both CP-even and CP-odd) has the phenomenology of the ScM, while the singlet has some extra terms from the

scalar potential with respect to just a pure singlet scalar. As the CP-odd scalar A can be a DM candidate, there are a few possible mass hierarchies:

- DM candidate = η_2 with $m_{\eta_2} < m_{\eta_1} < m_A$ or $m_{\eta_2} < m_A < m_{\eta_1}$;
- DM candidate = A with $m_A < m_{\eta_2} < m_{\eta_1}$.

In general, several (co-)annihilation channels are possible in the ScSM. All of these are included in micrOMEGAs v5.2.0 [54] which we use to compute the DM relic abundance. The DM abundance is required to be equal to or smaller than the *Planck* (2018) measured abundance [55]:

$$\Omega_{\rm DM}h^2 = 0.120 \pm 0.001. \tag{3.31}$$

Thus, the *Planck* measurement provides an upper limit on the DM relic abundance.

3.8 Direct detection

Direct detection (DD) typically imposes strong constraints on scalar DM candidates with a non-zero hypercharge due to the presence of t-channel Z/h-mediated diagrams [8]. The gauge interactions stem from the kinetic term for the doublet, namely

$$\mathcal{L} \supset (D_{\mu}\Phi)^{\dagger}(D^{\mu}\Phi)$$

$$\supset -\frac{g}{2\cos\theta_{W}}Z_{\mu}\left(\phi_{R}\partial^{\mu}A - A\partial^{\mu}\phi_{R}\right)$$

$$= -\frac{g}{2\cos\theta_{W}}Z_{\mu}\left[\cos\theta(\eta_{1}\partial^{\mu}A - A\partial^{\mu}\eta_{1}) - \sin\theta(\eta_{2}\partial^{\mu}A - A\partial^{\mu}\eta_{2})\right]. \tag{3.32}$$

Notice that the Z-mediated interactions are inelastic, and always involve a CP-even scalar and pseudoscalar A. A small enough mixing can suppress DD limits via the last term in eq. (3.32), as in this case, η_2 is mainly singlet and does not directly couple to the Z-boson. In addition, a large enough mass splitting (\gtrsim MeV) can kinematically forbid the scatterings between η_2 and A. This implies that $\lambda_{H\Phi,3} \gtrsim 10^{-6}$. Two cases are possible:

- 1. For $b \gg a$ (and $b \gg c$), η_2 is mainly doublet (with a correction proportional to κ) and the mass splitting with A is given by $\lambda_{H\Phi,3}$ (which can be made naturally smaller than in the ScM);
- 2. For $b \ll a$ (and $a \gg c$), η_2 is mainly singlet and m_A is given in terms of other parameters, so there is no reason for the mass splitting to be small, and thus inelastic scatterings are expected to be forbidden.

Interactions mediated by the SM Higgs h lead to the usual elastic (and also inelastic) spin-independent (SI) scattering; the resulting limits are also quite severe [56, 57], but they can be suppressed by small scalar couplings unlike in the case of Z-mediated interaction [58]. For non-zero mixing, the dimensionless h- η_2 - η_2 coupling is given by [28]

$$\lambda_{\text{eff}} \equiv \frac{1}{v} \left[\lambda_{H\varphi} v \cos^2 \theta - 2\kappa \sin \theta \cos \theta + \lambda_{123} v \sin^2 \theta \right] , \qquad (3.33)$$

where $\lambda_{123} \equiv \lambda_{H\Phi,1} + \lambda_{H\Phi,2} + \lambda_{H\Phi,3}$. As λ_{eff} decreases, the *h*-mediated direct detection cross section also decreases. This coupling will vanish (i.e., no overall h- η_2 - η_2 coupling) when the mixing angle satisfies the following relation:

$$\sin^2 \theta = \frac{(m_{\Phi}^2 - m_{\varphi}^2) + \lambda_{H\varphi} v^2 - \sqrt{(m_{\Phi}^2 - m_{\varphi}^2)^2 + \lambda_{123} \lambda_{H\varphi} v^4}}{2(m_{\Phi}^2 - m_{\varphi}^2) - \lambda_{123} v^2 + \lambda_{H\varphi} v^2},$$
(3.34)

We confirm that when the coupling $\lambda_{H\varphi}$ (λ_{123}) vanishes, the Higgs-DM coupling is zero only for pure singlet (doublet) DM. In the event that the couplings are exactly equal and dominate over the bare masses, $\lambda_{123} = \lambda_{H\varphi} \gg |m_{\Phi}^2 - m_{\varphi}^2|/v^2$, the effective Higgs coupling λ_{eff} vanishes for maximal mixing $\theta = \pi/4$.

Using micrOMEGAs, we compute the effective SI DM-proton scattering cross section, assuming that the local DM energy density scales proportional to the global one:

$$\sigma_{\text{eff}} \equiv \sigma_{\text{SI}}^p \cdot f_{\text{rel}} \,, \quad f_{\text{rel}} \equiv \Omega_X / \Omega_{\text{DM}} \,,$$
 (3.35)

where Ω_X is the X DM abundance $(X = \eta_2, A \text{ or } \psi_2)$ and Ω_{DM} is the *Planck* measured abundance in eq. (3.31). We then recast the observed exclusion limit from XENON1T [59] within micrOMEGAs [60] for a fixed DM mass and compare it against the effective SI cross section in eq. (3.35). There are a number of planned xenon-based experiments that will increase the sensitivity significantly, e.g., XENONnT [61], PandaX [62], LZ [63] and DARWIN [64]. In our plots, we will illustrate the expected reach of LZ only.

3.9 \mathbb{Z}_2 symmetry at high energies

The ScSM also has interesting features in light of the model viability up to high-energy scales [21, 65–67]. The trilinear coupling κ , due to the presence of the scalar singlet, gives positive contributions to the RGE evolution of the new scalar mass-squared parameters if it is real, thereby helping prevent the breaking of the model symmetries even in the absence of finite temperature effects. The compatibility with the evolution of the bare Higgs mass (and thus of EWSB) requires a separate study, which we leave for a future work. In principle, one could incorporate the evolution of Renormalisation Group Equations (RGEs) of model parameters into our numerical scan to verify that the \mathbb{Z}_2 symmetry remains unbroken at high-energy scales, but the practical implementation remains computationally difficult. Thus, we do not include RGE effects in our numerical analysis.

4 Numerical analysis

To efficiently sample the allowed parameter space of the ScSM, we use the Importance Nested Sampling algorithm implemented in MultiNest v3.10.0 [68] with 25,000 live points (nlive) and a stopping tolerance (tol) of 10^{-3} .8 The composite log-likelihood used is

$$\ln \mathcal{L}_{\text{total}}(\boldsymbol{\theta}) = \ln \mathcal{L}_{\kappa}(\boldsymbol{\theta}) + \ln \mathcal{L}_{\text{EWPT}}(\boldsymbol{\theta}) + \ln \mathcal{L}_{\mathcal{R}_{\gamma\gamma}}(\boldsymbol{\theta}) + \ln \mathcal{L}_{\text{LFV}}(\boldsymbol{\theta}) + \ln \mathcal{L}_{\Omega h^2}(\boldsymbol{\theta}) + \ln \mathcal{L}_{\text{DD}}(\boldsymbol{\theta}),$$
(4.1)

⁸As we will see in section 5, our fixed log-likelihood contours are mostly flat in the model parameter planes. For this reason, we run MultiNest with stringent settings to efficiently sample the 1σ and 2σ CL regions.

where θ are the free parameters of the ScSM. The individual log-likelihood contributions are described below:

- 1. $\ln \mathcal{L}_{\kappa}(\boldsymbol{\theta})$: log-likelihood for the trilinear coupling κ . It is Gaussian in nature, centered at 0 TeV with a standard deviation of 1.5 TeV, see eq. (3.7).
- 2. $\ln \mathcal{L}_{\text{EWPT}}(\boldsymbol{\theta})$: log-likelihood for the electroweak precision tests (EWPT) (see subsection 3.4). It is given by [69]

$$\ln \mathcal{L}_{\text{EWPO}}(\boldsymbol{\theta}) = -\frac{1}{2} \sum_{i,j} (\Delta \mathcal{O}_i - \overline{\Delta \mathcal{O}}_i) \left(\Sigma^2 \right)_{ij}^{-1} (\Delta \mathcal{O}_j - \overline{\Delta \mathcal{O}}_j), \tag{4.2}$$

where $\overline{\Delta O}_i$ are the central values for the shifts in eq. (3.25), $\Sigma_{ij}^2 \equiv \sigma_i \rho_{ij} \sigma_j$ is the covariance matrix, ρ_{ij} is the correlation matrix in eq. (3.26) and σ_i are the associated errors in eq. (3.25).

- 3. $\ln \mathcal{L}_{\mathcal{R}_{\gamma\gamma}}(\boldsymbol{\theta})$: log-likelihood for $R_{\gamma\gamma} \equiv \Gamma(h \to \gamma\gamma)_{\text{ScSM}}/\Gamma(h \to \gamma\gamma)_{\text{SM}}$ (see subsection 3.5). It is a Gaussian likelihood function, centered at the PDG measured value of 1.1 with a standard deviation of 0.1 [53]. The SM expectation is $\mathcal{R}_{\gamma\gamma} = 1.0$.
- 4. $\ln \mathcal{L}_{LFV}(\theta)$: log-likelihood for the LFV processes (see subsection 3.6). It is given by

$$\ln \mathcal{L}_{LFV}(\boldsymbol{\theta}) = \ln \mathcal{L}_{\mu \to e\gamma}(\boldsymbol{\theta}) + \ln \mathcal{L}_{\tau \to \mu\gamma}(\boldsymbol{\theta}) + \ln \mathcal{L}_{\tau \to e\gamma}(\boldsymbol{\theta}) + \ln \mathcal{L}_{\mu \to 3e}(\boldsymbol{\theta}) + \ln \mathcal{L}_{\tau \to 3\mu}(\boldsymbol{\theta}) + \ln \mathcal{L}_{\tau \to 3e}(\boldsymbol{\theta}) + \ln \mathcal{L}_{\mu \to e \text{ (Au)}}(\boldsymbol{\theta}) + \ln \mathcal{L}_{\mu \to e \text{ (Ti)}}(\boldsymbol{\theta}).$$
(4.3)

Each of the individual likelihood functions are Gaussian, and centered at a branching ratio/conversion rate of 0 with a standard deviation equal to the respective upper limit shown in column 2 of table 2.

- 5. $\ln \mathcal{L}_{\Omega h^2}(\boldsymbol{\theta})$: log-likelihood for the DM relic density Ωh^2 (see subsection 3.7). It is a one-sided Gaussian, i.e., a flat likelihood on $\Omega_X \leq \Omega_{\rm DM}$ and Gaussian for $\Omega_X > \Omega_{\rm DM}$. The *Planck* measured uncertainty is also combined in quadrature with a 5% theoretical uncertainty (stemming from our assumed uncertainty on the relic density calculation in micrOMEGAs).
- 6. $\ln \mathcal{L}_{DD}(\boldsymbol{\theta})$: log-likelihood for the XENON1T experiment (see subsection 3.8). It is a simple step-function-like likelihood, i.e., parameter points are allowed (rejected) if the effective SI cross section in eq. (3.35) is below (above) the official XENON1T exclusion limit [59] for a given DM mass.

The ranges and priors for the 21 (12 free + 9 nuisance) model parameters in normal ordering (NO) and inverted ordering (NO) are summarised in table 3.9 Due to the presence of coannihilations, we find it efficient to scan over δ_1 and δ_A (instead of m_{η_1} and m_A) where

$$\delta_1 \equiv m_{\eta_1} - m_{\eta_2} \,, \quad \delta_A \equiv m_A - m_{\eta_2} \,. \tag{4.4}$$

⁹We keep the CP-even $(m_{\eta_{1,2}})$ and CP-odd (m_A) scalar masses $\gtrsim 100\,\text{GeV}$ to avoid constraints from h/Z invisible decays and collider limits.

	Ranges	Priors
Model parameters		
$\{m_{\psi_1}, m_{\psi_2}\}$ (GeV)	$[10, 10^6]$	Log
$m_{\eta_2} ({ m GeV})$	$[100, 10^4]$	Log
$\delta_1 \equiv m_{\eta_1} - m_{\eta_2} (\text{GeV})$	$[10^{-3}, 10^4]$	Log
$\delta_A \equiv m_A - m_{\eta_2} (\text{GeV})$	$[-10^4, -10^{-3}] \cup [10^{-3}, 10^4]$	Log value
θ (rad.)	$[0,\pi]$	Flat
$\{\lambda_\Phi,\lambda_arphi\}$	$[10^{-3}, 4\pi]$	Log
$\{\lambda_{H\Phi,1},\lambda_{H\Phi,2},\lambda_{H\varphi},\lambda_{\Phi\varphi}\}$	$[-4\pi, -10^{-3}] \cup [10^{-3}, 4\pi]$	Log value
Nuisance parameters		
$\sin^2 \theta_{12}$	[0.275, 0.350]	Flat
$\sin^2 \theta_{13}$	[0.02044, 0.02435] (NO) [0.02064, 0.02457] (IO)	Flat
$\sin^2 \theta_{23}$	[0.433, 0.609] (NO) [0.436, 0.610] (IO)	Flat
$\frac{\Delta m_{21}^2}{10^{-5}\mathrm{eV}^2}$	[6.79, 8.01]	Flat
$\frac{\Delta m_{3l}^2}{10^{-3} \text{eV}^2}$	[2.436, 2.618] (NO) $[-2.601, -2.419]$ (IO)	Flat
$\delta_{ m CP}$ (°)	[144, 357] (NO) [205, 348] (IO)	Flat
$\alpha ({\rm rad.})$	$[0, 2\pi]$	Flat
$\{\zeta_1,\zeta_2\}$	$[10^{-3}, 10^3]$	Log

Table 3: Ranges and priors for 21 (12 free + 9 nuisance) model parameters. The parameters $\{\zeta_1, \zeta_2\}$ belong to the R matrix of the Casas-Ibarra parametrization [38] (see appendix B), whereas α is the Majorana phase in the PMNS matrix. The terms NO (IO) refer to Normal (Inverted) Ordering, whereas $\Delta m_{3l}^2 \equiv m_3^2 - m_1^2 > 0$ (NO) and $m_3^2 - m_2^2 < 0$ (IO).

By convention, $\delta_1 \geq 0$ as $m_{\eta_1} \geq m_{\eta_2}$. Meanwhile, $\delta_A > 0$ for η_2 as DM, $\delta_A < 0$ for A as DM, and either for ψ_2 as DM.

In the next section, we show various two-dimensional (2D) plots of the profile likelihood ratio (PLR) [70] in the relevant parameter planes or key observables of interest. Model

parameters that are not shown in those plots are profiled over, i.e., the composite log-likelihood function in eq. (4.1) is maximised with respect to those parameters. Using Wilks' theorem [71], the PLR can be used as a test statistic to approximately construct the 1σ ($\sim 68.3\%$) and 2σ ($\sim 95.4\%$) CL contours [72].

5 Results

We start by showing results for the scalar DM in the case of no mixing between the singlet and doublet (e.g., $\theta = 0$, $\pi/2$). For scalar doublet DM, we reproduce the standard results [73, 74]; we consider the CP-even scalar, but the results for the CP-odd scalar are similar. For singlet DM, we also reproduce the results from the literature [56, 57, 75, 76].¹⁰

Next, we turn on the mixing angle θ and consider separately the case of real scalar η_2 , real pseudoscalar A and Majorana fermion ψ_2 as DM candidates. We pay special attention on studying how the parameter space opens up in each cases with respect to the usual ScM.

5.1 No mixing case: Scotogenic model + scalar singlet

From eq. (2.7), the physical state η_2 in the case of no mixing is

$$\eta_2 \equiv \begin{cases}
\text{scalar singlet } \varphi \,, & \theta = 0 \,, \\
\text{scalar doublet } \phi_R \,, & \theta = \pi/2 \,.
\end{cases}$$
(5.1)

In both cases, the trilinear scalar coupling $\kappa = 0$, and the model reduces to the usual Scotogenic model plus a scalar singlet; we indeed recover the results from the literature.

In the left (right) panel of figure 2, we plot the η_2 relic density (effective SI η_2 scattering cross section with protons) versus the singlet DM η_2 mass for $\theta=0$. We see two allowed disconnected regions, at masses around 150 GeV and above \sim TeV. Notice that only in the latter region, the singlet can constitute 100% of the observed DM abundance [56]. As we see from the plot in the right panel, next-generation DD experiments will be able to test this model, given the fact that the quartic couplings are large enough to reproduce the abundance.

Similarly in figure 3, we plot the η_2 relic density (effective SI η_2 -p cross section) versus the CP-even doublet DM η_2 mass for $\theta=\pi/2.^{11}$ The upper left corner in the left plot implies a too-large annihilation cross-section to reproduce the observed DM abundance. Indeed, for the doublet DM to saturate the abundance, its mass should be $\gtrsim 500$ GeV. In this case, next-generation DD experiments will still leave a large portion of the parameter space unexplored. This is due to the fact that the annihilation cross section, driven by gauge interactions, is decoupled from the DD cross section (unless the mass splitting with the CP-odd scalar is \lesssim MeV).

¹⁰There is an extra parameter with respect to both models separately, $\lambda_{\Phi\varphi}$, but as expected, we see that it does not affect the model phenomenology.

¹¹Notice the under-sampling of the profile likelihood surface at small cross sections. This is expected due to the nature of our XENON1T likelihood (a step-function-like), i.e., parameter points have same likelihood if they are all compatible with the official XENON1T limit. A full coverage of this region requires a dedicated scan over extremely small h- η_2 - η_2 couplings, which is not the main goal of our study.

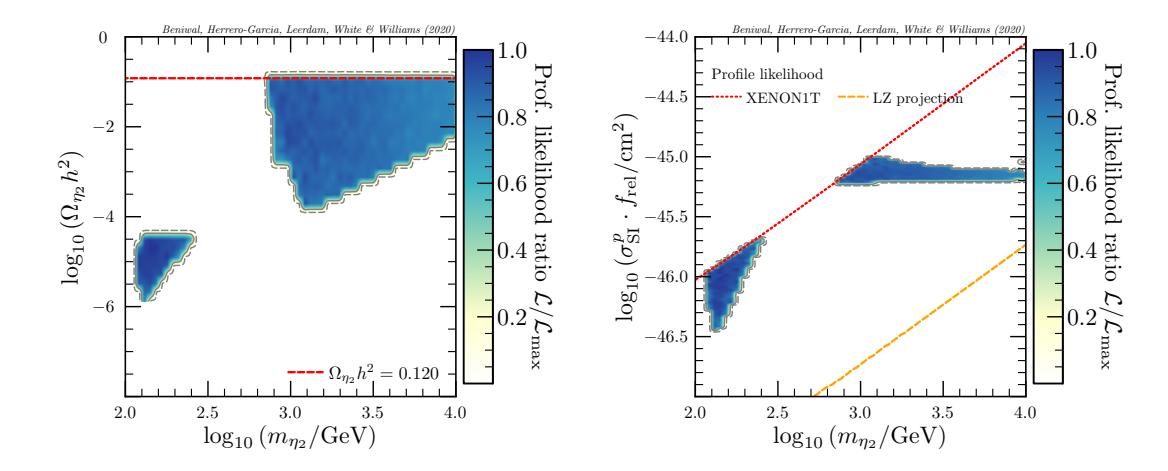


Figure 2: 2-dimensional (2D) plots of profile likelihood ratio (PLR) for the scalar singlet η_2 relic density (left panel) and spin-independent (SI) η_2 -proton direct detection (DD) cross section (right panel), scaled by the DM fraction, $f_{\rm rel} = \Omega_{\eta_2}/0.120$, for the case of $\theta = 0$ in Normal Ordering (NO). The dashed (dotted) red lines in the left (right) panel show the Planck measured DM abundance [55] (official XENON1T exclusion limit [59]), whereas the projected LZ sensitivity [77] is shown as dashed orange line in the right panel.

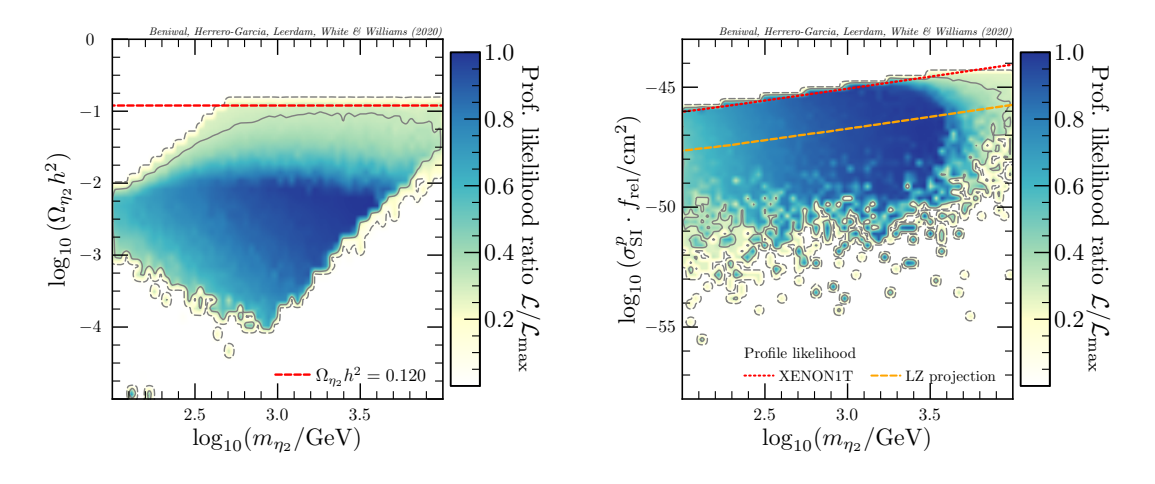


Figure 3: Same as figure 2, but for the case of $\theta = \pi/2$, i.e., pure scalar doublet DM.

5.2 DM candidate: real scalar, η_2

For the case of CP-even scalar DM η_2 with non-zero mixing, we find large regions in the model parameter space that can satisfy all included constraints. In figure 4, we plot some of the relevant parameters of interest; Normal ordering (NO) is always assumed, unless stated otherwise. In the top-left plot, we see the expected triangular-shaped region in the Yukawa couplings (plotted for the heaviest sterile singlet fermion ψ_1) vs $\lambda_{H\Phi,3}$. This stems from reproducing the observed neutrino masses. Small values of $\lambda_{H\Phi,3}$ demand large values for the Yukawa couplings, while for large $\lambda_{H\Phi,3}$ values, large values of the Yukawas are also somewhat possible, and compensated by the masses of the new particles. A somewhat

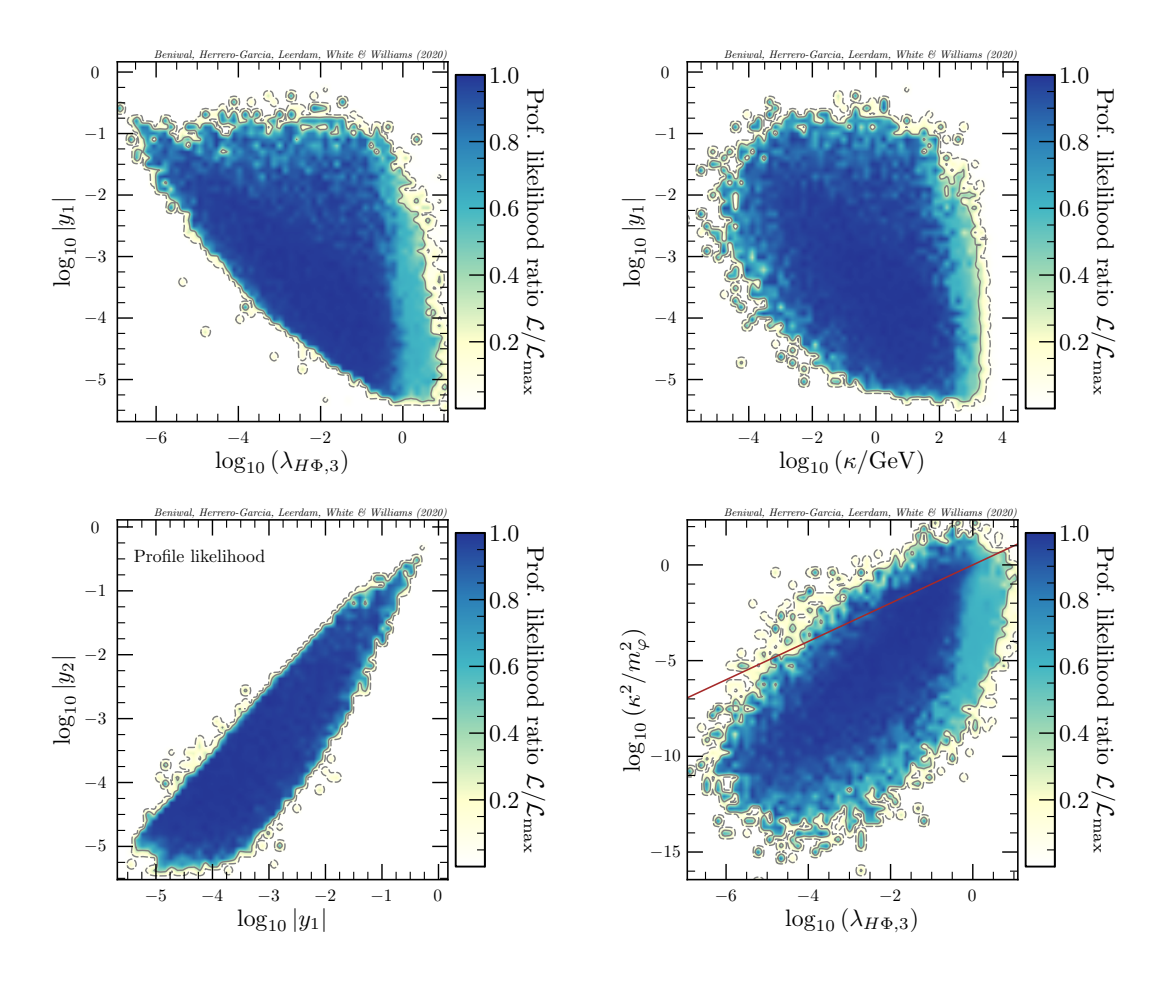


Figure 4: 2D plots of PLR in the planes of model parameters for the case of η_2 DM. In the bottom-right plot, the solid brown line corresponds to a 1:1 relationship between κ^2/m_{φ}^2 and $\lambda_{H\Phi,3}$.

similar structure is seen in the case of the trilinear coupling κ (top-right plot) for the same reasons, although in this case, the region is much less pronounced. In the bottom-left plot, we see how the Yukawa couplings are correlated amongst each other, with the heaviest sterile (y_1) being larger than the lightest one (y_2) ; this correlation becomes even more pronounced at large couplings. In the bottom-right plot, we observe how the ScSM demands a relationship between the trilinear and quartic couplings, such that neutrino masses are reproduced. This can be understood analytically in the limit of heavy scalar singlet masses, see eq. (3.16), as represented by a solid brown line in the plot.

In the top-left plot in figure 5, the η_2 abundance is much smaller for $m_{\eta_2} \sim m_h$ due to direct annihilation process $\eta_2 \eta_2 \to h h$. Final states with gauge bosons (W^+W^-/ZZ) are always open. Indeed, the dominant annihilation channels that determine the η_2 abundance involve gauge bosons, and less often the Higgs bosons. Annihilations into $t\bar{t}$, leptons or photons are sometimes present. When the scalar masses are degenerate enough, coannihilations can be important. An upper limit of $m_{\eta_2} \lesssim 5$ TeV is obtained at the 1σ CL, but is somewhat below the upper limit from the prior of 10 TeV. In the top-right plot, we

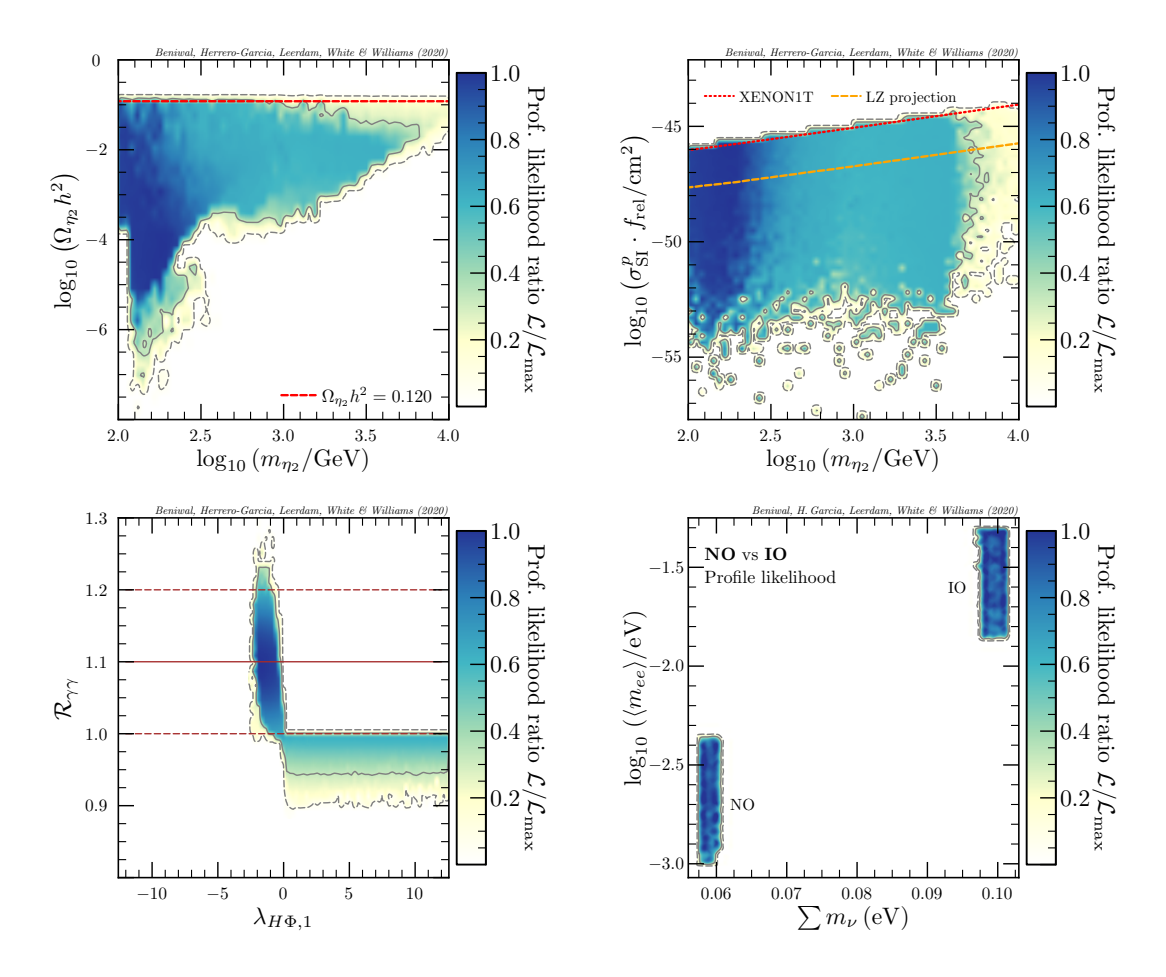


Figure 5: 2D plots of PLR for key observables of interest. Top-left and top-right plots: same as figure 2 but for η_2 DM with non-zero mixing. Bottom-left plot: solid (dashed) brown lines show the PDG central (standard deviation) value for $\mathcal{R}_{\gamma\gamma}$ of 1.1 (0.1). Bottom-right plot: $\langle m_{ee} \rangle$ vs $\sum m_{\nu}$ for Normal Ordering (NO) and Inverted Ordering (IO); see text for more details.

show the effective SI η_2 -proton scattering cross section. The rise in upper limit with DM mass is expected from the DM number density for heavier masses. The small cross sections arise from a cancellation in eq. (3.34); in any case, they are well below the sensitivity of next-generation DD experiments.

In the bottom-left plot in figure 5, we observe that the Higgs to di-photon rate with respect to the SM is enhanced (suppressed) for $\lambda_{H\Phi,1} < 0$ ($\lambda_{H\Phi,1} > 0$). It is evident that the currently allowed value, shown by horizontal brown lines, demands $\lambda_{H\Phi,1} < 0$. Finally, in the bottom-right plot, we show the effective neutrino mass parameter $\langle m_{ee} \rangle \equiv |\sum U_{ei}^2 m_i|$, which enters in the expression for the lifetime of neutrinoless double beta $(0\nu\beta\beta)$ decay [78]. As expected, we reproduce the expected result for NO and IO. In particular, IO results imply that $0.012\,\text{eV} \leq \langle m_{ee} \rangle \leq 0.05\,\text{eV}$. These values can potentially be tested in coming years, see refs. [79, 80] for recent reviews.

In the left panel of figure 6, we plot an LFV radiative decay versus the Yukawa of

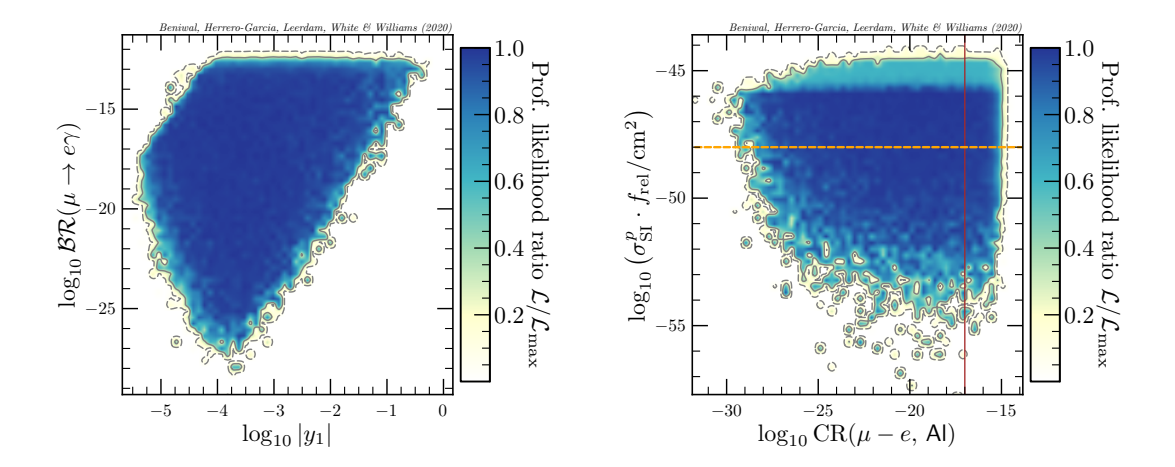


Figure 6: Left panel: LFV radiative decay versus the Yukawa of the heaviest fermion singlet. Right panel: SI DD cross section versus the $\mu \to e$ conversion rate in aluminium (AI). The solid brown (dashed orange) lines show the expected sensitivity of next-generation $\mu \to e$ conversion experiments (LZ projection for 50 GeV DM [77]).

the heaviest fermion singlet; here we observe a V-shaped region. The behaviour for large Yukawas goes as $\sim |y|^4$, as expected. For $|y_1| \lesssim 10^{-4}$, the contribution from other neutrino ($\propto |y_2|$) dominates. The upper-left region corresponds to $|y_2| \gg |y_1|$; we see that it is not allowed, as the mass of lightest fermion singlet is too light to suppress enough LFV. In the right panel of figure 6, we see how the next-generation DD experiments (e.g., LZ projected sensitivity for 50 GeV DM [77] – dashed orange line) test complementary parts of the parameter space to those of LFV experiments (e.g., expected sensitivity of $\mu - e$ conversion rate (an improvement by 4 orders of magnitude) – solid brown line).

We have checked that different LFV observables (see table 2) show a clear correlation among themselves. This is expected from the fact that Yukawa couplings are smaller than one, so that the box (dipole) contributions are suppressed (dominant):

$$\mathcal{BR}(\mu \to 3e) \simeq 6 \times 10^{-3} \,\mathcal{BR}(\mu \to e\gamma) \,,$$
 (5.2a)

$$CR(\mu - e, AI) \simeq 10^{-2} \mathcal{BR}(\mu \to e\gamma)$$
. (5.2b)

It is interesting to highlight that the sensitivity to $\mathcal{BR}(\mu \to 3e)$ is expected to improve by up to 4 orders of magnitude [81]. These conclusions have already been obtained in the literature, although for somewhat different versions of the model [11, 13, 22]. In addition, we have checked that there are no significant differences between the two mass orderings (NO vs IO).

In the left panel of figure 7, we show how the η_2 relic abundance changes with the dimensionless h- η_2 - η_2 coupling $\lambda_{\rm eff}$, see eq. (3.33). We observe how the smallest relic abundance is obtained for $\lambda_{\rm eff}$ values of order one, in which the annihilations proceed via a Higgs-mediated s-channel diagram. In the right panel, we see that the SI DD cross section scales linearly with $\lambda_{\rm eff}$, meaning that Z-mediated processes do not contribute significantly to the DD cross section.

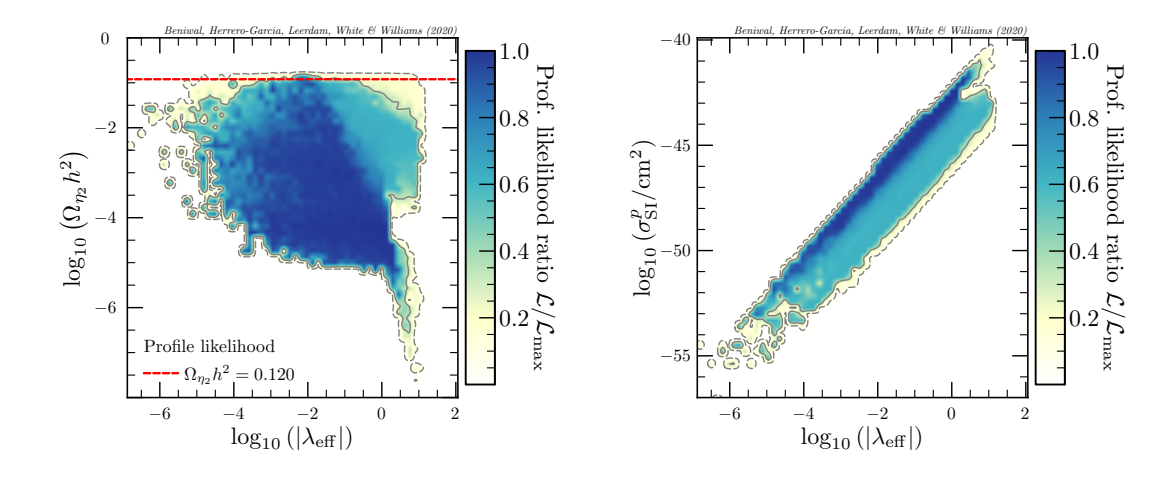


Figure 7: 2D plots of PLR for the η_2 relic abundance (*left panel*) and SI η_2 -proton cross section (*right panel*) versus the dimensionless h- η_2 - η_2 coupling, λ_{eff} , see eq. (3.33) for more details.

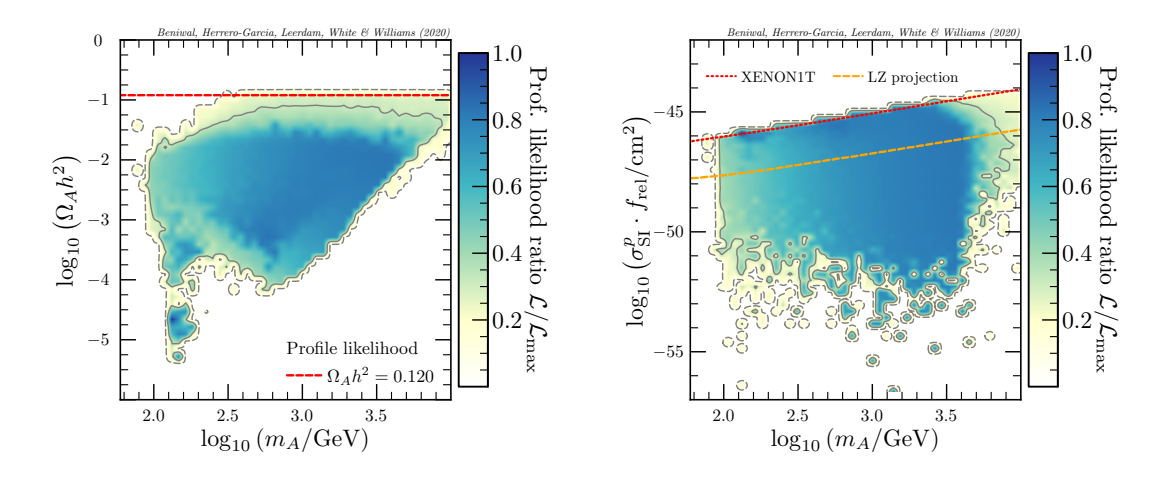


Figure 8: Same as figure 2 but for the case of real pseudoscalar A DM.

5.3 DM candidate: real pseudoscalar, A

The allowed parameter space and phenomenology of the ScSM in this case is similar to the real (CP-even) scalar coming from the doublet (see figure 3). The relic abundance of A is also bounded from above for low masses, as shown in the left panel of figure 8. This translates into a lower limit of $m_A \gtrsim 300 \,\text{GeV}$ for pseudoscalar A to saturate the observed DM abundance, somewhat smaller than for the CP-even candidate. This difference comes from the coupling $\lambda_{H\Phi,3}$, which enters differently into the scalar masses.

5.4 DM candidate: Majorana fermion, ψ_2

We do not investigate the case of fermion DM in detail, as it has already been explored in a model with similar phenomenology [22]. Here we simply confirm that we arrive at the same conclusions, namely that the fermion DM case requires coannihilations for its

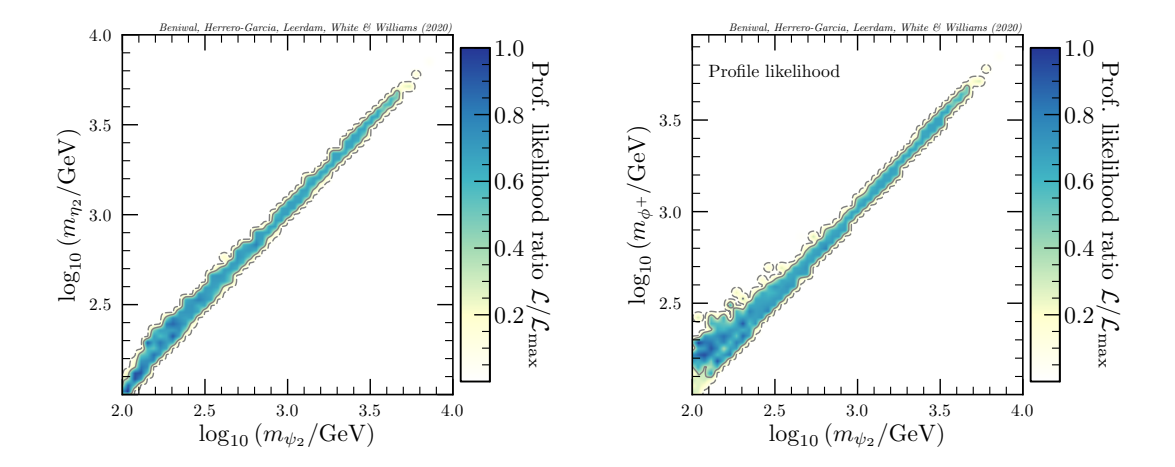


Figure 9: 2D plots of PLR in the case of ψ_2 DM. Both panels show the need for a mass degeneracy to saturate the observed DM abundance via coannihilations.

abundance to match the Planck measured value. In figure 9, we see that viable parameter space requires m_{ψ_2} to be degenerate with m_{η_2} (left panel) and m_{ϕ^+} (right panel). This is so because the scalar masses are set by similar combinations of Lagrangian parameters, and EWPT demands them to be close in mass, although there is somewhat a wider region at small masses for the charged scalar. Thus, the case of fermion DM in the ScSM introduces a fine-tuning that is not present in the case of scalar DM. Apart from this difference, the Yukawa couplings and LFV processes are similar to the case of η_2 and A DM. In regards to DD in the Scotogenic model with a fermion singlet, it occurs at one-loop level, and is typically suppressed [9, 22, 82, 83].

6 Conclusions

We have proposed a simple variation of the original Scotogenic Model (ScM), namely with an extra real scalar singlet. The model, termed the ScotoSinglet Model (ScSM), is arguably the simplest extension of the popular ScM, with a very rich phenomenology and several interesting features:

- 1. It allows for DM to be scalar (CP even or odd) with a naturally-suppressed direct detection rate, either due to a typically large mass splitting with the opposite-CP scalar (not only dependent on $\lambda_{H\Phi,3}$ as in ScM), or due to a small mixing, $\theta \simeq 0$. In this case, DM is mainly singlet with a small doublet component, and Z-boson mediated interactions are suppressed;
- 2. There are two contributions to neutrino masses: the usual Scotogenic one ($\propto \lambda_{H\Phi,3}$) and the new singlet one ($\propto \kappa^2$). In principle, lepton number violation (e.g., the smallness of neutrino masses) demands both couplings to be small, which is technically natural. However, in the limit of large singlet mass, a large $\lambda_{H\Phi,3}$ can be cancelled with the trilinear coupling term ($\propto \kappa^2/m_{\omega}^2$), see eq. (3.16). This allows for the cou-

plings to be larger than usual and contribute to the DM phenomenology, e.g., to DM annihilations and scatterings.

3. The presence of the singlet improves the stability of the \mathbb{Z}_2 symmetry up to highenergy scales when the trilinear coupling κ is real, as it contributes positively to the evolution of Renormalisation Group Equations (RGEs) for m_{φ}^2 and m_{Φ}^2 .

The above features significantly open up the parameter space with respect to the ScM. Extensions to three sterile fermions are not expected to change our results significantly. Other variations, such a proper RGE study, or a Generalised ScotoSinglet Model [22], is left out for a future work.

The origin of neutrino masses, the nature of DM, and their possible connection remains an open question that may possibly take several decades to fully understand. While we wait eagerly for a positive signal, the study of simplified models (such as the ScSM) allows us to gain insight into the big puzzles, and search for new correlations among different observables that can help us in distinguishing models among a plethora of possibilities.

Acknowledgments

We thank Arcadi Santamaria and Céline Degrande for helpful discussions. AB is supported by fund for Scientific Research F.N.R.S. through the F.6001.19 convention. JHG is supported by the Generalitat Valenciana through the GenT Excellence Program (CIDE-GENT/2020/020). NL, MW, and AGW are supported by the Australian Research Council (ARC) Centre of Excellence for Particle Physics at the Terascale (CoEPP) (CE110001104) and the ARC Discovery Project grant DP180102209.

Computational resources have been provided by the Consortium des Équipements de Calcul Intensif (CÉCI), funded by the Fonds de la Recherche Scientifique de Belgique (F.R.S.-FNRS) under Grant No. 2.5020.11 and by the Walloon Region. We acknowledge the use of pippi v2.0 [84] for generating our 2-dimensional profile likelihood ratio plots.

A Mass eigenstate basis

For the weak eigenstates $\mathcal{A} = (\phi_R, \varphi)^T$, the mass-term is given by

$$\mathscr{L}_{\text{mass-term}} = -\frac{1}{2} \mathcal{A}^T \mathcal{M}^2 \mathcal{A}, \qquad (A.1)$$

where

$$\mathcal{M}^{2} = \begin{pmatrix} \frac{\partial^{2} V}{\partial \phi_{R}^{2}} & \frac{\partial^{2} V}{\partial \phi_{R} \partial \varphi} \\ \frac{\partial^{2} V}{\partial \varphi \partial \phi_{R}} & \frac{\partial^{2} V}{\partial \varphi^{2}} \end{pmatrix} = \begin{pmatrix} a & c \\ c & b \end{pmatrix}$$
(A.2)

is a (non-diagonal) squared mass matrix. To diagonalise \mathcal{M}^2 , we define the mass eigenstates (η_1, η_2) as

$$\begin{pmatrix} \eta_1 \\ \eta_2 \end{pmatrix} = \begin{pmatrix} \cos \theta & \sin \theta \\ -\sin \theta & \cos \theta \end{pmatrix} \begin{pmatrix} \phi_R \\ \varphi \end{pmatrix} , \tag{A.3}$$

where θ is the mixing angle. Thus,

$$\begin{pmatrix} \phi_R \\ \varphi \end{pmatrix} = \mathcal{O} \begin{pmatrix} \eta_1 \\ \eta_2 \end{pmatrix}, \quad \mathcal{O} = \begin{pmatrix} \cos \theta - \sin \theta \\ \sin \theta & \cos \theta \end{pmatrix}. \tag{A.4}$$

In the mass eigenstate basis, a squared mass matrix satisfies the following relation:

$$\mathcal{O}^T \mathcal{M}^2 \mathcal{O} = \mathcal{D} \equiv \begin{pmatrix} m_{\eta_1}^2 & 0\\ 0 & m_{\eta_2}^2 \end{pmatrix}. \tag{A.5}$$

Following the analysis in appendix B of ref. [85], we find that

$$m_m^2 = a\cos^2\theta + b\sin^2\theta + c\sin 2\theta, \qquad (A.6a)$$

$$m_{\eta_2}^2 = a\sin^2\theta + b\cos^2\theta - c\sin 2\theta, \qquad (A.6b)$$

$$0 = -\frac{1}{2}(a-b)\sin 2\theta + c\cos 2\theta, \qquad (A.6c)$$

where the last equality can also be expressed as

$$\tan 2\theta = \frac{2c}{a-b} \,. \tag{A.7}$$

In matrix notation, the above expressions read as

$$\begin{pmatrix}
m_{\eta_1}^2 \\
m_{\eta_2}^2 \\
0
\end{pmatrix} = \begin{pmatrix}
\cos^2 \theta & \sin^2 \theta & 2\sin \theta \cos \theta \\
\sin^2 \theta & \cos^2 \theta & -2\sin \theta \cos \theta \\
-\sin \theta \cos \theta & \sin \theta \cos \theta & \cos^2 \theta - \sin^2 \theta
\end{pmatrix} \begin{pmatrix} a \\ b \\ c \end{pmatrix}.$$
(A.8)

By taking $\theta \to -\theta$, we can express (a, b, c) in terms of $(m_{\eta_1}^2, m_{\eta_2}^2, \theta)$ as

$$a = m_{\eta_1}^2 \cos^2 \theta + m_{\eta_2}^2 \sin^2 \theta,$$
 (A.9a)

$$b = m_{\eta_1}^2 \sin^2 \theta + m_{\eta_2}^2 \cos^2 \theta \,, \tag{A.9b}$$

$$c = (m_{n_1}^2 - m_{n_2}^2)\sin\theta\cos\theta$$
. (A.9c)

Using the relations for (a, b, c) from section 2, we get

$$m_{\Phi}^2 = m_{\eta_1}^2 \cos^2 \theta + m_{\eta_2}^2 \sin^2 \theta - \frac{1}{2} (\lambda_{H\Phi,1} + \lambda_{H\Phi,2} + \lambda_{H\Phi,3}) v^2, \qquad (A.10a)$$

$$m_{\varphi}^2 = m_{\eta_1}^2 \sin^2 \theta + m_{\eta_2}^2 \cos^2 \theta - \frac{1}{2} \lambda_{H\varphi} v^2,$$
 (A.10b)

$$\kappa = \frac{1}{v} (m_{\eta_1}^2 - m_{\eta_2}^2) \sin \theta \cos \theta.$$
 (A.10c)

B Parameterisation of the Yukawa couplings

Following the working in the original Casas-Ibarra paper [38] (see also ref. [86] for a one-loop parametrization, and ref. [87] for a general parametrization), we write the neutrino mass matrix in terms of our high energy parameters, equivalent to eq. (3.9), as

$$M_{\nu} = f y^T \hat{M} y \,, \tag{B.1}$$

where $f = 1/(32\pi^2)$, y is a 2 × 3 matrix of Yukawa couplings and $\hat{M} = \text{diag}(\hat{m}_1, \hat{m}_2)$ with

$$\hat{m}_k = m_{\psi_k} \left[\cos^2 \theta \, F_k(\eta_1) + \sin^2 \theta \, F_k(\eta_2) - F_k(A) \right],$$
 (B.2)

where the loop function is given in eq. (3.10).

The neutrino mass matrix can also be written in terms of the physical neutrino masses (m_1, m_2, m_3) and unitary PMNS matrix U as

$$U^T M_{\nu} U = D_{\nu} \,, \tag{B.3}$$

where $D_{\nu} = \text{diag}(m_1, m_2, m_3)$; in our model with two fermion singlets, $m_1 = 0$ for NO and $m_3 = 0$ for IO. The neutrino mass eigenstates ν_i (i = 1, 2, 3) are related to the neutrino flavour eigenstates ν_{α} $(\alpha = e, \mu, \tau)$ by

$$\nu_{\alpha} = \sum_{i=1}^{3} U_{\alpha i} \nu_{i} . \tag{B.4}$$

Now, we can write $D_{\nu} = fU^T y^T \hat{M} y U$, and pre- and post-multiply with $D_{-1/2}$ and $D_{-1/2}^T$, respectively, to get

$$I_{2\times 2} = f D_{-1/2} U^T y^T \hat{M}^{1/2T} \hat{M}^{1/2} y U D_{-1/2}^T,$$
(B.5)

where

$$D_{\pm 1/2} \equiv \begin{cases} \begin{pmatrix} 0 & m_2^{\pm 1/2} & 0 \\ 0 & 0 & m_3^{\pm 1/2} \end{pmatrix}, & \text{NO}, \\ \begin{pmatrix} m_1^{\pm 1/2} & 0 & 0 \\ 0 & m_2^{\pm 1/2} & 0 \end{pmatrix}, & \text{IO}. \end{cases}$$
(B.6)

We define an orthogonal 2×2 matrix R as

$$R \equiv \sqrt{f} \,\hat{M}^{1/2} \, y \, U \, D_{-1/2}^T \,, \tag{B.7}$$

such that

$$y = \frac{1}{\sqrt{f}} \,\hat{M}^{-1/2} \, R \, D_{1/2} \, U^{\dagger} \,. \tag{B.8}$$

		Normal Ordering (best fit)		Inverted Ordering ($\Delta \chi^2 = 10.4$)	
		bfp $\pm 1\sigma$	3σ range	bfp $\pm 1\sigma$	3σ range
	$\sin^2 \theta_{12}$	$0.310^{+0.013}_{-0.012}$	$0.275 \rightarrow 0.350$	$0.310^{+0.013}_{-0.012}$	$0.275 \rightarrow 0.350$
data	$\theta_{12}/^{\circ}$	$33.82^{+0.78}_{-0.76}$	$31.61 \rightarrow 36.27$	$33.82^{+0.78}_{-0.75}$	$31.61 \rightarrow 36.27$
	$\sin^2 \theta_{23}$	$0.563^{+0.018}_{-0.024}$	$0.433 \rightarrow 0.609$	$0.565^{+0.017}_{-0.022}$	$0.436 \rightarrow 0.610$
atmospheric	$\theta_{23}/^{\circ}$	$48.6^{+1.0}_{-1.4}$	$41.1 \rightarrow 51.3$	$48.8^{+1.0}_{-1.2}$	$41.4 \rightarrow 51.3$
tmo	$\sin^2 \theta_{13}$	$0.02237^{+0.00066}_{-0.00065}$	$0.02044 \to 0.02435$	$0.02259^{+0.00065}_{-0.00065}$	$0.02064 \to 0.02457$
SK 8	$\theta_{13}/^{\circ}$	$8.60^{+0.13}_{-0.13}$	$8.22 \rightarrow 8.98$	$8.64^{+0.12}_{-0.13}$	$8.26 \rightarrow 9.02$
with	$\delta_{\mathrm{CP}}/^{\circ}$	221^{+39}_{-28}	$144 \rightarrow 357$	282^{+23}_{-25}	$205 \rightarrow 348$
	$\frac{\Delta m_{21}^2}{10^{-5} \text{ eV}^2}$	$7.39^{+0.21}_{-0.20}$	$6.79 \rightarrow 8.01$	$7.39_{-0.20}^{+0.21}$	$6.79 \rightarrow 8.01$
	$\frac{\Delta m_{3\ell}^2}{10^{-3} \text{ eV}^2}$	$+2.528^{+0.029}_{-0.031}$	$+2.436 \to +2.618$	$-2.510^{+0.030}_{-0.031}$	$-2.601 \rightarrow -2.419$

Table 4: Neutrino oscillation parameters from Nu-FIT v4.1 (2019) [88, 89].

It is easy to check that this satisfies the low energy definition by substituting back into the high energy expression. We parametrise the R matrix as

$$R \equiv \begin{pmatrix} \cos(\zeta_1 + i\zeta_2) & \sin(\zeta_1 + i\zeta_2) \\ -\sin(\zeta_1 + i\zeta_2) & \cos(\zeta_1 + i\zeta_2) \end{pmatrix}$$

$$= \begin{pmatrix} \cos\zeta_1 \cosh\zeta_2 - i\sin\zeta_1 \sinh\zeta_2 & \sin\zeta_1 \cosh\zeta_2 + i\cos\zeta_1 \sinh\zeta_2 \\ -\sin\zeta_1 \cosh\zeta_2 - i\cos\zeta_1 \sinh\zeta_2 & \cos\zeta_1 \cosh\zeta_2 - i\sin\zeta_1 \sinh\zeta_2 \end{pmatrix}, \quad (B.9)$$

where $\zeta_1, \zeta_2 \in \mathbb{R}$. In our numerical scans, we use the standard parametrisation for $U = (u_1, u_2, u_3)$ for one massless neutrino, namely

$$U = \begin{pmatrix} c_{12}c_{13} & s_{12}c_{13} & s_{13}e^{-i\delta_{\text{CP}}} \\ -s_{12}c_{23} - c_{12}s_{23}s_{13}e^{i\delta_{\text{CP}}} & c_{12}c_{23} - s_{12}s_{23}s_{13}e^{i\delta_{\text{CP}}} & s_{23}c_{13} \\ s_{12}s_{23} - c_{12}c_{23}s_{13}e^{i\delta_{\text{CP}}} & -c_{12}s_{23} - s_{12}c_{23}s_{13}e^{i\delta_{\text{CP}}} & c_{23}c_{13} \end{pmatrix} \begin{pmatrix} 1 & 0 & 0 \\ 0 & e^{i\alpha} & 0 \\ 0 & 0 & 1 \end{pmatrix},$$
(B.10)

where $c_{ij} \equiv \cos \theta_{ij}$ and $s_{ij} \equiv \sin \theta_{ij}$ (θ_{12} , θ_{13} , and θ_{23} are the 3 lepton mixing angles), α ($\delta_{\rm CP}$) is the Majorana (Dirac) phase. As the lightest neutrino is massless with just two fermionic singlets, there is only one physical Majorana phase. For the neutrino oscillation parameters, we use the results based on a global fit from the Nu-FIT collaboration [88, 89] with SK atmospheric data (see table 4).

C Potential stability

We follow the analysis in refs. [90, 91]. We parameterise

$$H^{\dagger}H = \frac{1}{2}h_1^2, \quad \Phi^{\dagger}\Phi = \frac{1}{2}h_2^2, \quad \varphi^2 = h_3^2, \quad H^{\dagger}\Phi = \frac{1}{2}h_1h_2\rho_{12}e^{i\phi_{12}}.$$
 (C.1)

The quartic part of the potential now reads

$$V_{4} = \lambda_{H}(H^{\dagger}H)^{2} + \lambda_{\Phi}(\Phi^{\dagger}\Phi)^{2} + \frac{\lambda_{\varphi}}{4}\varphi^{4} + \lambda_{H\Phi,1}(H^{\dagger}H)(\Phi^{\dagger}\Phi)$$

$$+ \lambda_{H\Phi,2}(H^{\dagger}\Phi)(\Phi^{\dagger}H) + \frac{1}{2}\lambda_{H\Phi,3}[(H^{\dagger}\Phi)^{2} + \text{H.c.}] + \frac{1}{2}\lambda_{H\varphi}(H^{\dagger}H)\varphi^{2} + \frac{1}{2}\lambda_{\Phi\varphi}(\Phi^{\dagger}\Phi)\varphi^{2}$$

$$= \left(h_{1}^{2} h_{2}^{2} h_{3}^{2}\right) \begin{pmatrix} a_{11} & a_{12} & a_{13} \\ a_{12} & a_{22} & a_{23} \\ a_{13} & a_{23} & a_{33} \end{pmatrix} \begin{pmatrix} h_{1}^{2} \\ h_{2}^{2} \\ h_{3}^{2} \end{pmatrix}, \qquad (C.2)$$

where

$$a_{11} = \frac{1}{4}\lambda_H$$
, $a_{22} = \frac{1}{4}\lambda_{\Phi}$, $a_{33} = \frac{1}{4}\lambda_{\varphi}$, $a_{13} = \frac{1}{8}\lambda_{H\varphi}$, $a_{23} = \frac{1}{8}\lambda_{\Phi\varphi}$, (C.3a)

$$a_{12} = \frac{1}{8} \left[\lambda_{H\Phi,1} + \rho_{12}^2 \left(\lambda_{H\Phi,2} + \lambda_{H\Phi,3} \cos(2\phi_{12}) \right) \right].$$
 (C.3b)

The potential is minimised with respect to ρ_{12} and ϕ_{12} by setting

$$\cos(2\phi_{12}) = \begin{cases} -1, & \lambda_{H\Phi,3} > 0, \\ 1, & \lambda_{H\Phi,3} < 0, \end{cases} \qquad \rho_{12} = \begin{cases} 0, & \lambda_{H\Phi,2} - |\lambda_{H\Phi,3}| > 0, \\ 1, & \lambda_{H\Phi,2} - |\lambda_{H\Phi,3}| < 0. \end{cases}$$
(C.4)

The co-positivity conditions are given by

$$\{\lambda_H, \lambda_\Phi, \lambda_\varphi\} \ge 0,$$
 (C.5a)

$$c_1 \equiv \frac{1}{2} \left[\lambda_{H\Phi,1} + \rho_{12}^2 (\lambda_{H\Phi,2} - |\lambda_{H\Phi,3}|) \right] + \sqrt{\lambda_H \lambda_\Phi} \ge 0,$$
 (C.5b)

$$c_2 \equiv \frac{1}{2}\lambda_{H\varphi} + \sqrt{\lambda_H \lambda_{\varphi}} \ge 0,$$
 (C.5c)

$$c_3 \equiv \frac{1}{2} \lambda_{\Phi\varphi} + \sqrt{\lambda_{\Phi} \lambda_{\varphi}} \ge 0,$$
 (C.5d)

$$\sqrt{\lambda_H \lambda_{\Phi} \lambda_{\varphi}} + \frac{1}{2} \left[\lambda_{H\Phi,1} + \rho_{12}^2 (\lambda_{H\Phi,2} - |\lambda_{H\Phi,3}|) \right] \sqrt{\lambda_{\varphi}}
+ \frac{1}{2} \lambda_{H\varphi} \sqrt{\lambda_{\Phi}} + \frac{1}{2} \lambda_{\Phi\varphi} \sqrt{\lambda_H} + \sqrt{2c_1 c_2 c_3} \ge 0.$$
(C.5e)

D Renormalisation Group Equations (RGEs)

Here we provide the Renormalisation Group Equations (RGEs) for the ScSM at one-loop level, as computed using the SARAH package [92].

D.1 Gauge couplings

$$\beta_{g_1}^{(1)} = \frac{21}{5}g_1^3, \qquad \beta_{g_2}^{(1)} = -3g_2^3, \qquad \beta_{g_3}^{(1)} = -7g_3^3.$$
 (D.1)

D.2 Quartic scalar couplings

$$\begin{split} \beta_{\lambda H}^{(1)} &= \frac{27}{200} g_1^4 + \frac{9}{20} g_1^2 g_2^2 + \frac{9}{8} g_2^4 - \frac{9}{5} g_1^2 \lambda_H - 9 g_2^2 \lambda_H + 24 \lambda_H^2 + 2 \lambda_{H\Phi,1}^2 + 2 \lambda_{H\Phi,1} \lambda_{H\Phi,2} \\ &\quad + \lambda_{H\Phi,2}^2 + \lambda_{H\Phi,3}^2 + \frac{1}{2} \lambda_{H\varphi}^2 + 12 \lambda_H \text{Tr} \Big(Y_d Y_d^\dagger \Big) + 4 \lambda_H \text{Tr} \Big(Y_c Y_c^\dagger \Big) + 12 \lambda_H \text{Tr} \Big(Y_u Y_u^\dagger \Big) \\ &\quad - 6 \text{Tr} \Big(Y_d Y_d^\dagger Y_d Y_d^\dagger \Big) - 2 \text{Tr} \Big(Y_c Y_c^\dagger Y_c Y_c^\dagger \Big) - 6 \text{Tr} \Big(Y_u Y_u^\dagger Y_u Y_u^\dagger \Big) \,, \\ &\quad - 6 \text{Tr} \Big(Y_d Y_d^\dagger Y_d Y_d^\dagger \Big) - 2 \text{Tr} \Big(Y_c Y_c^\dagger Y_c Y_c^\dagger \Big) - 6 \text{Tr} \Big(Y_u Y_u^\dagger Y_u Y_u^\dagger \Big) \,, \\ &\quad - 6 \text{Tr} \Big(Y_d Y_d^\dagger Y_d Y_d^\dagger \Big) - 2 \text{Tr} \Big(Y_c Y_c^\dagger Y_c Y_c^\dagger \Big) - 6 \text{Tr} \Big(Y_u Y_u^\dagger Y_u Y_u^\dagger \Big) \,, \\ &\quad - 6 \text{Tr} \Big(Y_d Y_d^\dagger Y_d Y_d^\dagger \Big) - 2 \text{Tr} \Big(Y_u Y_u^\dagger Y_u Y_u^\dagger \Big) \,, \\ &\quad - 9 g_2^2 \lambda_\Phi + 24 \lambda_\Phi^2 + \frac{1}{2} \lambda_{\Phi\varphi}^2 + 2 \lambda_{H\Phi,1}^2 + 2 \lambda_{H\Phi,1} \lambda_{H\Phi,2} + \lambda_{H\Phi,2}^2 + \lambda_{H\Phi,3}^2 - \frac{9}{5} g_1^2 \lambda_\Phi \\ &\quad - 9 g_2^2 \lambda_\Phi + 24 \lambda_\Phi^2 + \frac{1}{2} \lambda_{\Phi\varphi}^2 + 4 \lambda_\Phi \text{Tr} \Big(Y_u Y_\psi^\dagger \Big) - 2 \text{Tr} \Big(Y_u Y_\psi^\dagger Y_u Y_\psi^\dagger \Big) \,, \\ &\quad - 9 g_2^2 \lambda_\Phi + 24 \lambda_\Phi^2 + \frac{1}{2} \lambda_{\Phi\varphi}^2 + 4 \lambda_\Phi \text{Tr} \Big(Y_u Y_\psi^\dagger \Big) - 2 \text{Tr} \Big(Y_u Y_\psi^\dagger Y_u Y_\psi^\dagger \Big) \,, \\ &\quad - 9 g_1^2 \lambda_\Phi + 2 \lambda_{\Phi}^2 + \frac{9}{2} g_1^2 \lambda_{H\Phi,1} + 9 g_2^2 \lambda_{H\Phi,1} + 12 \lambda_H \lambda_{H\Phi,2} + 4 \lambda_{H\Phi,1}^2 + 4 \lambda_{H\Phi,2}^2 +$$

D.3 Yukawas, masses and trilinear couplings

$$\beta_{Y_{\psi}}^{(1)} = \frac{1}{2} \left(3Y_{\psi} Y_{\psi}^{\dagger} Y_{\psi} + Y_{\psi} Y_{e}^{\dagger} Y_{e} \right) + Y_{\psi} \left[-\frac{9}{20} \left(5g_{2}^{2} + g_{1}^{2} \right) + \text{Tr} \left(Y_{\psi} Y_{\psi}^{\dagger} \right) \right], \tag{D.10}$$

$$\beta_{m_{\psi}}^{(1)} = m_{\psi} Y_{\psi}^* Y_{\psi}^T + Y_{\psi} Y_{\psi}^{\dagger} m_{\psi} , \qquad (D.11)$$

$$\beta_{\kappa}^{(1)} = -\frac{9}{10}g_1^2\kappa - \frac{9}{2}g_2^2\kappa + 2\kappa\lambda_{H\Phi,1} + 4\kappa\lambda_{H\Phi,2} + 6\kappa\lambda_{H\Phi,3} + 2\kappa\lambda_{H\varphi} + 2\kappa\lambda_{\Phi\varphi} + 3\kappa\mathrm{Tr}\left(Y_dY_d^{\dagger}\right) + \kappa\mathrm{Tr}\left(Y_eY_e^{\dagger}\right) + \kappa\mathrm{Tr}\left(Y_\psi Y_\psi^{\dagger}\right) + 3\kappa\mathrm{Tr}\left(Y_u Y_u^{\dagger}\right), \tag{D.12}$$

$$\beta_{\mu_H^2}^{(1)} = -2\kappa^2 - \frac{9}{10}g_1^2\mu_H^2 - \frac{9}{2}g_2^2\mu_H^2 + 12\lambda_H\mu_H^2 - 4\lambda_{H\Phi,1}m_{\Phi}^2 - 2\lambda_{H\Phi,2}m_{\Phi}^2 - \lambda_{H\varphi}m_{\varphi}^2$$

$$6\mu_H^2 \text{Tr}\left(Y_d Y_d^{\dagger}\right) + 2\mu_H^2 \text{Tr}\left(Y_e Y_e^{\dagger}\right) + 6\mu_H^2 \text{Tr}\left(Y_u Y_u^{\dagger}\right), \tag{D.13}$$

$$\beta_{m_{\Phi}^{2}}^{(1)} = 2\kappa^{2} - 4\lambda_{H\Phi,1}\mu_{H}^{2} - 2\lambda_{H\Phi,2}\mu_{H}^{2} - \frac{9}{10}g_{1}^{2}m_{\Phi}^{2} - \frac{9}{2}g_{2}^{2}m_{\Phi}^{2} + 12\lambda_{\Phi}m_{\Phi}^{2} + \lambda_{\Phi\varphi}m_{\varphi}^{2} + 2m_{\Phi}^{2}\mathrm{Tr}\left(Y_{\psi}Y_{\psi}^{\dagger}\right) - 4\mathrm{Tr}\left(m_{\psi}Y_{\psi}Y_{\psi}^{\dagger}m_{\psi}\right), \tag{D.14}$$

$$\beta_{m_{\varphi}^{(1)}}^{(1)} = 8\kappa^2 - 4\lambda_{H\varphi}\mu_H^2 + 4\lambda_{\Phi\varphi}m_{\Phi}^2 + 6\lambda_{\varphi}m_{\varphi}^2.$$
 (D.15)

Note that in our convention, $\mu_H^2 > 0$. As we can see from the last two equations, for real values of κ , it contributes positively to the running of the bare squared-masses of the \mathbb{Z}_2 odd scalars, but negatively to the Higgs doublet bare squared-mass term.

References

- [1] S. M. Boucenna, S. Morisi and J. W. Valle, The low-scale approach to neutrino masses, Adv. High Energy Phys. 2014 (2014) 831598, [1404.3751].
- [2] Y. Cai, J. Herrero-García, M. A. Schmidt, A. Vicente and R. R. Volkas, From the trees to the forest: a review of radiative neutrino mass models, Front. in Phys. 5 (2017) 63, [1706.08524].
- [3] E. Ma, Verifiable radiative seesaw mechanism of neutrino mass and dark matter, Phys. Rev. D 73 (2006) 077301, [hep-ph/0601225].
- [4] J. Kubo, E. Ma and D. Suematsu, Cold Dark Matter, Radiative Neutrino Mass, $\mu \to e\gamma$, and Neutrinoless Double Beta Decay, Phys. Lett. B **642** (2006) 18–23, [hep-ph/0604114].
- [5] D. Aristizabal Sierra, J. Kubo, D. Restrepo, D. Suematsu and O. Zapata, Radiative seesaw: Warm dark matter, collider and lepton flavour violating signals, Phys. Rev. D 79 (2009) 013011, [0808.3340].
- [6] G. B. Gelmini, E. Osoba and S. Palomares-Ruiz, *Inert-Sterile Neutrino: Cold or Warm Dark Matter Candidate*, *Phys. Rev. D* 81 (2010) 063529, [0912.2478].
- [7] D. Suematsu, T. Toma and T. Yoshida, Reconciliation of CDM abundance and mu $-\dot{\epsilon}$ e gamma in a radiative seesaw model, Phys. Rev. D 79 (2009) 093004, [0903.0287].
- [8] T. Hambye, F. S. Ling, L. Lopez Honorez and J. Rocher, Scalar Multiplet Dark Matter, JHEP 07 (2009) 090, [0903.4010].
- [9] D. Schmidt, T. Schwetz and T. Toma, Direct Detection of Leptophilic Dark Matter in a Model with Radiative Neutrino Masses, Phys. Rev. D 85 (2012) 073009, [1201.0906].

- [10] J. Racker, Mass bounds for baryogenesis from particle decays and the inert doublet model, JCAP 1403 (2014) 025, [1308.1840].
- [11] T. Toma and A. Vicente, Lepton Flavor Violation in the Scotogenic Model, JHEP **01** (2014) 160, [1312.2840].
- [12] E. Molinaro, C. E. Yaguna and O. Zapata, FIMP realization of the scotogenic model, JCAP 1407 (2014) 015, [1405.1259].
- [13] A. Vicente and C. E. Yaguna, Probing the scotogenic model with lepton flavor violating processes, JHEP 02 (2015) 144, [1412.2545].
- [14] A. Ahriche, K. L. McDonald and S. Nasri, The Scale-Invariant Scotogenic Model, JHEP 06 (2016) 182, [1604.05569].
- [15] A. G. Hessler, A. Ibarra, E. Molinaro and S. Vogl, Probing the scotogenic FIMP at the LHC, JHEP 01 (2017) 100, [1611.09540].
- [16] I. M. Ávila, V. De Romeri, L. Duarte and J. W. Valle, Minimalistic scotogenic scalar dark matter, Eur. Phys. J. C 80 (2020) 908, [1910.08422].
- [17] A. Ahriche, A. Jueid and S. Nasri, Radiative neutrino mass and Majorana dark matter within an inert Higgs doublet model, Phys. Rev. D 97 (2018) 095012, [1710.03824].
- [18] A. Ahriche, A. Arhrib, A. Jueid, S. Nasri and A. de La Puente, Mono-Higgs Signature in the Scotogenic Model with Majorana Dark Matter, Phys. Rev. D 101 (2020) 035038, [1811.00490].
- [19] S. Baumholzer, V. Brdar, P. Schwaller and A. Segner, Shining Light on the Scotogenic Model: Interplay of Colliders and Cosmology, JHEP 09 (2020) 136, [1912.08215].
- [20] L. Sarma, P. Das and M. K. Das, Scalar dark matter and leptogenesis in the minimal scotogenic model, Nucl. Phys. B 963 (2021) 115300, [2004.13762].
- [21] P. Escribano, M. Reig and A. Vicente, Generalizing the Scotogenic model, JHEP 07 (2020) 097, [2004.05172].
- [22] C. Hagedorn, J. Herrero-García, E. Molinaro and M. A. Schmidt, Phenomenology of the Generalised Scotogenic Model with Fermionic Dark Matter, JHEP 11 (2018) 103, [1804.04117].
- [23] Y. Farzan, A minimal model linking two great mysteries: neutrino mass and dark matter, Phys. Rev. D 80 (2009) 073009, [0908.3729].
- [24] D. Restrepo, O. Zapata and C. E. Yaguna, Models with radiative neutrino masses and viable dark matter candidates, JHEP 11 (2013) 011, [1308.3655].
- [25] F. Bonnet, M. Hirsch, T. Ota and W. Winter, Systematic study of the d=5 Weinberg operator at one-loop order, JHEP 07 (2012) 153, [1204.5862].
- [26] J. Alcaide, D. Das and A. Santamaria, A model of neutrino mass and dark matter with large neutrinoless double beta decay, JHEP 04 (2017) 049, [1701.01402].
- [27] S. Esch, M. Klasen and C. E. Yaguna, A singlet doublet dark matter model with radiative neutrino masses, JHEP 10 (2018) 055, [1804.03384].
- [28] T. Cohen, J. Kearney, A. Pierce and D. Tucker-Smith, Singlet-Doublet Dark Matter, Phys. Rev. D 85 (2012) 075003, [1109.2604].

- [29] C. Cheung and D. Sanford, Simplified Models of Mixed Dark Matter, JCAP **02** (2014) 011, [1311.5896].
- [30] A. Dutta Banik and D. Majumdar, Inert doublet dark matter with an additional scalar singlet and 125 GeV Higgs boson, Eur. Phys. J. C 74 (2014) 3142, [1404.5840].
- [31] A. Ahriche, A. Jueid and S. Nasri, A natural scotogenic model for neutrino mass & dark matter, Phys. Lett. B 814 (2021) 136077, [2007.05845].
- [32] T. Hugle, M. Platscher and K. Schmitz, Low-Scale Leptogenesis in the Scotogenic Neutrino Mass Model, Phys. Rev. D 98 (2018) 023020, [1804.09660].
- [33] T. Alanne, T. Hugle, M. Platscher and K. Schmitz, Low-scale leptogenesis assisted by a real scalar singlet, JCAP 03 (2019) 037, [1812.04421].
- [34] T. Hashimoto and D. Suematsu, Inflation and DM phenomenology in a scotogenic model extended with a real singlet scalar, Phys. Rev. D 102 (2020) 115041, [2009.13057].
- [35] C. Bonilla, L. M. de la Vega, J. Lamprea, R. A. Lineros and E. Peinado, Fermion Dark Matter and Radiative Neutrino Masses from Spontaneous Lepton Number Breaking, New J. Phys. 22 (2020) 033009, [1908.04276].
- [36] A. Alloul, N. D. Christensen, C. Degrande, C. Duhr and B. Fuks, FeynRules 2.0 A complete toolbox for tree-level phenomenology, Comput. Phys. Commun. 185 (2014) 2250–2300, [1310.1921].
- [37] A. Belyaev, N. D. Christensen and A. Pukhov, CalcHEP 3.4 for collider physics within and beyond the Standard Model, Comput. Phys. Commun. 184 (2013) 1729–1769, [1207.6082].
- [38] J. A. Casas and A. Ibarra, Oscillating neutrinos and muon \rightarrow e, gamma, Nucl. Phys. B **618** (2001) 171–204, [hep-ph/0103065].
- [39] J. Herrero-Garca, T. Ohlsson, S. Riad and J. Wirn, Full parameter scan of the Zee model: exploring Higgs lepton flavor violation, JHEP 04 (2017) 130, [1701.05345].
- [40] J. A. Casas, D. G. Cerdeo, J. M. Moreno and J. Quilis, Reopening the Higgs portal for single scalar dark matter, JHEP 05 (2017) 036, [1701.08134].
- [41] M. S. Bilenky and A. Santamaria, One loop effective Lagrangian for a standard model with a heavy charged scalar singlet, Nucl. Phys. B 420 (1994) 47–93, [hep-ph/9310302].
- [42] J. Elias-Miro, J. R. Espinosa, G. F. Giudice, H. M. Lee and A. Strumia, *Stabilization of the Electroweak Vacuum by a Scalar Threshold Effect*, *JHEP* **06** (2012) 031, [1203.0237].
- [43] M. E. Peskin and T. Takeuchi, Estimation of oblique electroweak corrections, Phys. Rev. D 46 (Jul, 1992) 381–409.
- [44] M. E. Peskin and T. Takeuchi, New constraint on a strongly interacting higgs sector, Phys. Rev. Lett. 65 (Aug, 1990) 964–967.
- [45] H. E. Haber and D. O'Neil, Basis-independent methods for the two-Higgs-doublet model III: The CP-conserving limit, custodial symmetry, and the oblique parameters S, T, U, Phys. Rev. D 83 (2011) 055017, [1011.6188].
- [46] G. Passarino and M. J. G. Veltman, One Loop Corrections for e^+e^- Annihilation Into $\mu^+\mu^-$ in the Weinberg Model, Nucl. Phys. B **160** (1979) 151–207.
- [47] R. Barbieri, L. J. Hall and V. S. Rychkov, *Improved naturalness with a heavy Higgs: An Alternative road to LHC physics*, *Phys. Rev. D* **74** (2006) 015007, [hep-ph/0603188].

- [48] J. Haller, A. Hoecker, R. Kogler, K. Mönig, T. Peiffer and J. Stelzer, Update of the global electroweak fit and constraints on two-Higgs-doublet models, Eur. Phys. J. C 78 (2018) 675, [1803.01853].
- [49] J. R. Ellis, M. K. Gaillard and D. V. Nanopoulos, A Phenomenological Profile of the Higgs Boson, Nucl. Phys. B 106 292.
- [50] M. A. Shifman, A. I. Vainshtein, M. B. Voloshin and V. I. Zakharov, Low-Energy Theorems for Higgs Boson Couplings to Photons, Sov. J. Nucl. Phys. 30 (1979) 711–716.
- [51] M. Carena, I. Low and C. E. M. Wagner, Implications of a Modified Higgs to Diphoton Decay Width, JHEP 08 (2012) 060, [1206.1082].
- [52] MEG collaboration, A. Baldini et al., Search for the lepton flavour violating decay $\mu^+ \to e^+ \gamma$ with the full dataset of the MEG experiment, Eur. Phys. J. C 76 (2016) 434, [1605.05081].
- [53] PARTICLE DATA GROUP collaboration, M. Tanabashi et al., Review of Particle Physics, Phys. Rev. D 98 (2018) 030001.
- [54] G. Bélanger, F. Boudjema, A. Goudelis, A. Pukhov and B. Zaldivar, micrOMEGAs5.0: Freeze-in, Comput. Phys. Commun. 231 (2018) 173–186, [1801.03509].
- [55] Planck collaboration, N. Aghanim et al., Planck 2018 results. VI. Cosmological parameters, Astron. Astrophys. 641 (2020) A6, [1807.06209].
- [56] P. Athron, J. M. Cornell, F. Kahlhoefer, J. Mckay, P. Scott and S. Wild, *Impact of vacuum stability, perturbativity and XENON1T on global fits of* \mathbb{Z}_2 *and* \mathbb{Z}_3 *scalar singlet dark matter, Eur. Phys. J. C* **78** (2018) 830, [1806.11281].
- [57] GAMBIT collaboration, P. Athron et al., Global analyses of Higgs portal singlet dark matter models using GAMBIT, Eur. Phys. J. C 79 (2019) 38, [1808.10465].
- [58] M. Escudero, A. Berlin, D. Hooper and M.-X. Lin, *Toward (Finally!) Ruling Out Z and Higgs Mediated Dark Matter Models*, *JCAP* 12 (2016) 029, [1609.09079].
- [59] XENON collaboration, E. Aprile et al., Dark Matter Search Results from a One Ton-Year Exposure of XENON1T, Phys. Rev. Lett. 121 (2018) 111302, [1805.12562].
- [60] G. Bélanger, A. Mjallal and A. Pukhov, Recasting direct detection limits within micrOMEGAs and implication for non-standard Dark Matter scenarios, Eur. Phys. J. C 81 (2021) 239, [2003.08621].
- [61] XENON1T collaboration, E. Aprile et al., Conceptual design and simulation of a water Cherenkov muon veto for the XENON1T experiment, JINST 9 (2014) P11006, [1406.2374].
- [62] PANDAX-II collaboration, X. Cui et al., Dark Matter Results From 54-Ton-Day Exposure of PandaX-II Experiment, Phys. Rev. Lett. 119 (2017) 181302, [1708.06917].
- [63] LZ collaboration, D. Akerib et al., LUX-ZEPLIN (LZ) Conceptual Design Report, 1509.02910.
- [64] DARWIN collaboration, J. Aalbers et al., DARWIN: towards the ultimate dark matter detector, JCAP 11 (2016) 017, [1606.07001].
- [65] A. Merle and M. Platscher, Parity Problem of the Scotogenic Neutrino Model, Phys. Rev. D 92 (2015) 095002, [1502.03098].
- [66] A. Merle and M. Platscher, Running of radiative neutrino masses: the scotogenic model—revisited, JHEP 11 (2015) 148, [1507.06314].

- [67] M. Lindner, M. Platscher, C. E. Yaguna and A. Merle, Fermionic WIMPs and vacuum stability in the scotogenic model, Phys. Rev. D 94 (2016) 115027, [1608.00577].
- [68] F. Feroz, M. Hobson and M. Bridges, MultiNest: an efficient and robust Bayesian inference tool for cosmology and particle physics, Mon. Not. Roy. Astron. Soc. 398 (2009) 1601–1614, [0809.3437].
- [69] S. Profumo, M. J. Ramsey-Musolf, C. L. Wainwright and P. Winslow, Singlet-catalyzed electroweak phase transitions and precision Higgs boson studies, Phys. Rev. D 91 (2015) 035018, [1407.5342].
- [70] K. Cranmer, Statistical Challenges for Searches for New Physics at the LHC, in Statistical Problems in Particle Physics, Astrophysics and Cosmology (L. Lyons and M. Karagöz Ünel, eds.), p. 112, Jan, 2006. physics/0511028. DOI.
- [71] S. Wilks, The Large-Sample Distribution of the Likelihood Ratio for Testing Composite Hypotheses, Annals Math. Statist. 9 (1938) 60–62.
- [72] G. Cowan, K. Cranmer, E. Gross and O. Vitells, Asymptotic formulae for likelihood-based tests of new physics, Eur. Phys. J. C 71 (2011) 1554, [1007.1727].
- [73] L. Lopez Honorez, E. Nezri, J. F. Oliver and M. H. Tytgat, *The Inert Doublet Model: An Archetype for Dark Matter*, *JCAP* **02** (2007) 028, [hep-ph/0612275].
- [74] M. Gustafsson, S. Rydbeck, L. Lopez-Honorez and E. Lundstrom, Status of the Inert Doublet Model and the Role of multileptons at the LHC, Phys. Rev. D 86 (2012) 075019, [1206.6316].
- [75] C. Burgess, M. Pospelov and T. ter Veldhuis, *The Minimal model of nonbaryonic dark matter: A Singlet scalar*, *Nucl. Phys. B* **619** (2001) 709–728, [hep-ph/0011335].
- [76] J. M. Cline, K. Kainulainen, P. Scott and C. Weniger, Update on scalar singlet dark matter, Phys. Rev. D 88 (2013) 055025, [1306.4710].
- [77] LUX-ZEPLIN collaboration, D. Akerib et al., Projected WIMP sensitivity of the LUX-ZEPLIN dark matter experiment, Phys. Rev. D 101 (2020) 052002, [1802.06039].
- [78] W. Rodejohann, Neutrinoless double beta decay and neutrino physics, J. Phys. G 39 (2012) 124008, [1206.2560].
- [79] S. Dell'Oro, S. Marcocci, M. Viel and F. Vissani, Neutrinoless double beta decay: 2015 review, Adv. High Energy Phys. 2016 (2016) 2162659, [1601.07512].
- [80] M. J. Dolinski, A. W. Poon and W. Rodejohann, Neutrinoless Double-Beta Decay: Status and Prospects, Ann. Rev. Nucl. Part. Sci. 69 (2019) 219–251, [1902.04097].
- [81] A. Blondel et al., Research Proposal for an Experiment to Search for the Decay $\mu \to eee$, 1301.6113.
- [82] A. Ibarra, C. E. Yaguna and O. Zapata, Direct Detection of Fermion Dark Matter in the Radiative Seesaw Model, Phys. Rev. D 93 (2016) 035012, [1601.01163].
- [83] J. Herrero-Garcia, E. Molinaro and M. A. Schmidt, Dark matter direct detection of a fermionic singlet at one loop, Eur. Phys. J. C 78 (2018) 471, [1803.05660].
- [84] P. Scott, Pippi painless parsing, post-processing and plotting of posterior and likelihood samples, Eur. Phys. J. Plus 127 (2012) 138, [1206.2245].
- [85] A. Beniwal, M. Lewicki, M. White and A. G. Williams, Gravitational waves and electroweak baryogenesis in a global study of the extended scalar singlet model, JHEP **02** (2019) 183, [1810.02380].

- [86] J. Lopez-Pavon, E. Molinaro and S. Petcov, Radiative Corrections to Light Neutrino Masses in Low Scale Type I Seesaw Scenarios and Neutrinoless Double Beta Decay, JHEP 11 (2015) 030, [1506.05296].
- [87] I. Cordero-Carrión, M. Hirsch and A. Vicente, General parametrization of Majorana neutrino mass models, Phys. Rev. D 101 (2020) 075032, [1912.08858].
- [88] I. Esteban, M. C. Gonzalez-Garcia, A. Hernandez-Cabezudo, M. Maltoni and T. Schwetz, Global analysis of three-flavour neutrino oscillations: synergies and tensions in the determination of θ_{23} , δ_{CP} , and the mass ordering, JHEP **01** (2019) 106, [1811.05487].
- [89] I. Esteban, C. Garcia, A. Cabezudo, M. Maltoni and T. Schwetz, "NuFIT 4.1." http://www.nu-fit.org, 2019.
- [90] K. Kannike, Vacuum Stability Conditions From Copositivity Criteria, Eur. Phys. J. C 72 (2012) 2093, [1205.3781].
- [91] K. Kannike, Vacuum Stability of a General Scalar Potential of a Few Fields, Eur. Phys. J. C 76 (2016) 324, [1603.02680].
- [92] F. Staub, SARAH, 0806.0538.